Annual Report April 1, 2014 - March 31, 2015

journal or publication title	University of Tsukuba Tandem Accelerator Complex (UTTAC) Annual Report
number	2014
year	2015
URL	http://hdl.handle.net/2241/00145858

UTTAC-84, 2015

UTTAC

ANNUAL REPORT 2014

TANDEM ACCELERATOR COMPLEX
Research Facility Center for Science and Technology
University of Tsukuba

http://www.tac.tsukuba.ac.jp/

UTTAC

ANNUAL REPORT 2014

April 1, 2014 – March 31, 2015

UTTAC-84, 2015

Executive Editor : Eiji Kita
Editors : Daiichiro Sekiba, Tetsuaki Moriguchi, Kimikazu Sasa,Yoshihiro Yamato
and Aya Kashifuku

UTTAC ANNUAL REPORT is a series of issues, which include annual reports of
Tandem Accelerator Complex, Research Facility Center
for Science and Technology, University of Tsukuba.

Tandem Accelerator Complex, Research Facility Center for Science and Technology,
University of Tsukuba
Tennodai 1-1-1, Tsukuba, Ibaraki 305-8577, Japan

annual@tac.tsukuba.ac.jp

PREFACE

This annual report covers research conducted at the Tandem Accelerator Complex(TAC), Research Facility Center for Science and Technology, University of Tsukuba, during fiscal year(FY) 2014 (April 1, 2014–March 31, 2015). After the Great East Japan Earthquake on March 11, 2011, research has been limited to that using the 1 MV Tandetron accelerator and radiation source experiments, ^{57}Co Mössbauer spectroscopy, and positron annihilation spectroscopy. According to our original plan, we would have finished reconstruction by the end of FY2014, and a new 6 MV accelerator would have started operation. However, since we needed to finish the removal procedure at first, the reconstruction of the main accelerator was postponed. The circumstances of our research has therefore still not changed much from the last fiscal year. Thus, this volume has slightly fewer pages as compared to older volumes like the one for last year.

A new 6 MV tandem-type accelerator with support from the government arrived in mid-March 2014 at the TAC from the National Electrostatics Corporation in Middleton, Wisconsin, USA. We are hoping for future research activities after the removal of the old accelerator.

The efforts of the Open Advanced Facilities Initiative supported by Ministry of Education, Culture, Sports, Science and Technology (MEXT) were continued in this term. The government assisted additional facilities related to this program with an extra budget. With this support, accelerated performance in this program was achieved. We are very much looking forward to operating and reporting on the new 6 MV accelerator.

Editors

CONTENTS

1.

ACCELERATOR AND FACILITIES

1.1 Accelerator operation 2014

K. Sasa, S. Ishii, H. Kimura, H. Oshima, Y. Tajima, T. Takahashi, Y. Yamato,
D. Sekiba, T. Moriguchi, E. Kita

The University of Tsukuba Tandem Accelerator Complex (UTTAC) is a major center of ion beam research in Japan. We have operated and maintained the 1 MV Tandetron accelerator, the 1 MV high-resolution Rutherford back scattering (RBS) system and the radio-isotope utilization equipment. At present, the 6 MV Pelletron tandem accelerator system has been designed and constructed at the university as part of the post-quake reconstruction project.

The total service time of the UTTAC multi-tandem accelerator facility was 2,512 hours in the fiscal year 2014. 816 hours for accelerators and 54 days for the radio-isotope utilization equipment were used under the project "Promotion of Advanced R&D Facility Utilization", which was supported financially by the Ministry of Education, Culture, Sports, Science and Technology (MEXT) of JAPAN. In the project, a total of 17 research programs were conducted in 2014.

1 MV Tandetron accelerator

The operating time and the experimental beam time of the 1 MV Tandetron accelerator were 671.4 and 228.1 hours, respectively, during the total service time in 2014. A total of 50 research programs were carried out and a total of 499 researchers used the 1 MV Tandetron accelerator. Figure 1 shows the percentage of accelerated ions for the 1 MV Tandetron accelerator. Figure 2 shows the percentage of research fields for the 1 MV Tandetron accelerator in 2014.

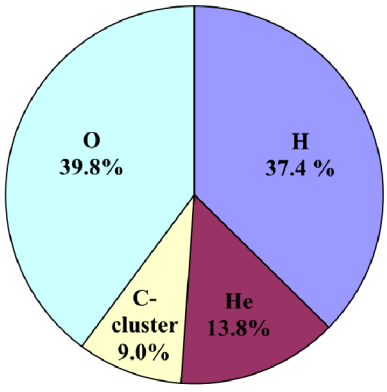

Fig. 1. Percentage of accelerated ions for the 1 MV Tandetron accelerator in 2014.

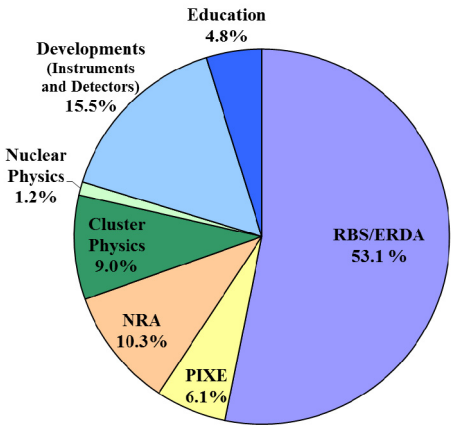

Fig. 2. Percentage of research fields for the 1 MV Tandetron accelerator in 2014.

6 MV Pelletron tandem accelerator

We planned to install the new horizontal-type 6 MV Pelletron tandem accelerator in the experimental room on the first floor to replace the damaged 12UD Pelletron tandem accelerator by the Great East Japan Earthquake of 11 March 2011 [1]. A three-year plan for the new accelerator's construction was started in 2012. The 6 MV Pelletron tandem accelerator will be used for various ion-beam research projects, such as

AMS, microbeam applications, particle-induced X-ray emission (PIXE) analysis for geoscience and materials research, heavy ion RBS and elastic recoil detection analysis, nuclear reaction analysis for hydrogen in materials, and high-energy ion irradiation for semiconductor and nuclear physics. All experimental equipment is installed on the first floor at UTTAC. Only rooms for control and data analysis are on the second floor. Figure 3 gives an overview of the equipment on the first floor. The new accelerator system consists of the 6 MV Pelletron tandem accelerator, four new ion sources, the Lamb-shift polarized ion source (S1 in Fig. 3), and five new beam courses. After the 105° analyzer magnet, the beam line is separated in two directions by the 40° switching magnet in the accelerator room. A high-energy beam transport line equipped with a vertical ion-irradiation system is connected from the accelerator room to the existing experimental room, which houses seven beam courses. A total of 12 beam courses will be available for nuclear physics, ion beam applications, and AMS.

The Lamb-shift polarized ion source was used as the injector of polarized proton and deuteron beams to the old tandem accelerator on the 9th floor at UTTAC [2]. After the earthquake, this ion source was moved to a new experimental building outside the accelerator building. In the accelerator room, there are four negative-ion sources. In Fig. 3, S2 is a high-current Cs-sputtering negative-ion source (SNICS II), and S3 is a radio frequency charge exchange ion source (Alphatros) to produce He^- beams for injection into the 6 MV Pelletron tandem accelerator. S4 and S5 are the multi-cathode Cs-sputtering negative-ion sources (MC-SNICSs) for AMS.

In the accelerator room, the ion beam analysis (IBA) system equipped with a high-precision five-axis goniometer is located on the L1 beam course. The L2 beam course has a large environmental testing chamber (1 m diameter) that will be mainly used for the radiation-tolerance testing of semiconductor devices for space satellites. The L3 beam course is constructed as follows: the Oxford microbeams quadrupole lens system [3] is used to obtain spot diameters of the order of 1 μm and below, and a superconducting detector [4] is used for high-sensitivity PIXE analysis. The L4 beam course is the rare-particle detection system for AMS. The L5 beam course is a general-purpose line for ion beam applications. In the experimental room, there are two large magnetic spectrographs (A6 and A7 beam courses) for nuclear physics. Other beam lines are used for ion beam channeling (A2 beam course), 3D fabrications with swift heavy ions (A3 beam course), and hydrogen analysis (A4 beam course). There is also a large general-purpose chamber (A5 beam course).

The 6 MV Pelletron tandem accelerator was installed in the spring of 2014 at the University of Tsukuba. Routine beam delivery and experiments will start in 2015.

References

[1] K. Sasa, Proceedings of HIAT 2012, Joint Accelerator Conferences Website (2012) 80–82.

[2] Y. Tagishi, J. Sanada, Nucl. Instr. Meth 164 (1979) 411–413.

[3] G. W. Grime, F. Watt, Nucl. Instr. Meth B 30 (1988) 227–234.

[4] M. Ohkubo, S. Shiki, M. Ukibe, N. Matsubayashi, Y. Kitajima, S. Nagamachi, Scientific Reports 2 (2012) article number:831.

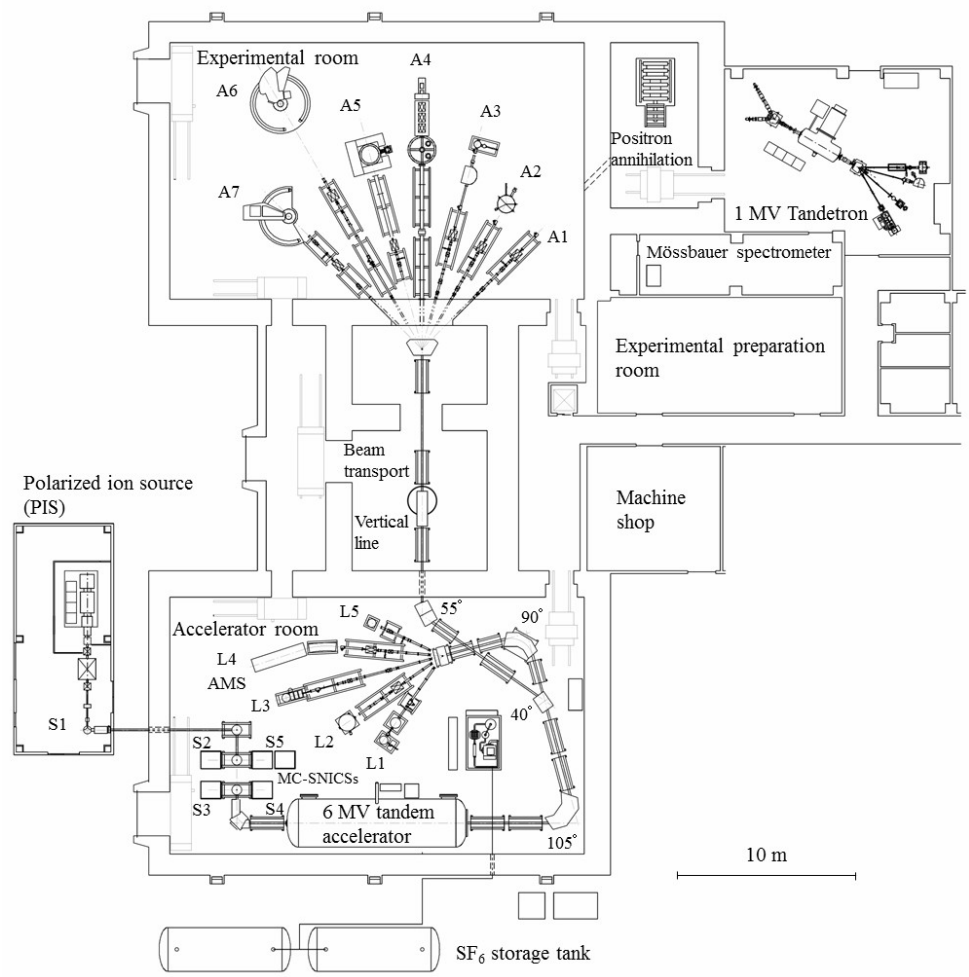

Fig. 3. Overall view of the first floor at UTTAC. The 6 MV Pelletron tandem accelerator and its beam lines, the 1 MV Tandetron accelerator, and a positron-annihilation spectrometry system are set up on the first floor.

Fig. 4. Photograph of the 6 MV Pelletron tandem accelerator under construction in the accelerator room.

2.

NUCLEAR PHYSICS

1.2 Performance prediction of the new Tsukuba AMS system

K. Sasa, T. Takahashi, M. Matsumura, T. Matsunaka, Y. Satou, D. Izumi, K. Sueki

Fig. 1 details the Tsukuba 6 MV AMS system [1]. It has two Cs sputtering negative ion sources for AMS: a 40-sample MC-SNICS for the routine measurement of all nuclides and a hybrid source with a 39-sample MC-SNICS equipped with a CO_2 gas introduction system [2] manufactured by NEC with either graphite or CO_2 samples. It is expected to achieve ultra-small-scale ^{14}C AMS measurements of 10 μg C. At the low-energy side, the injection energy from the ion sources is 65 keV. The 90° high-mass-resolution double-focusing magnetic analyzer with a 457 mm radius has a mass energy product of ME/Z^2 = 15 amu MeV. A 15 kV pulsed power supply is provided to bias the 90° magnetic analyzer chamber for the sequential injection of up to four different beams with a maximum mass difference of 17%. The main accelerator (model 18SDH-2 Pelletron, NEC) has a long gas stripper tube assembly and a foil changer with 80 foil holders for equilibrium stripping ions. Carbon stripper foils will be mainly used for ^{36}Cl AMS to obtain chlorine ions in a high charge state. The stripper gas canal is about 10 mm in diameter and 95 cm long. The rare-particle detection system is set on the −20° port on the switching magnet. A 22.5° ESA (3.81 m radius) is provided to filter out unwanted ions whose mass energy product (ME/Z^2) is the same as the rare isotope of interest. Only ions with the correct energy-to-charge-state ratios (E/Z) will pass through the ESA, which has a resolution of $E/\Delta E$ = 200. A five-electrode gas ionization detector is installed on the end station of the rare-particle detection system, which is similar in design to the gas ionization detector on the AMS system of the SUERC [3].

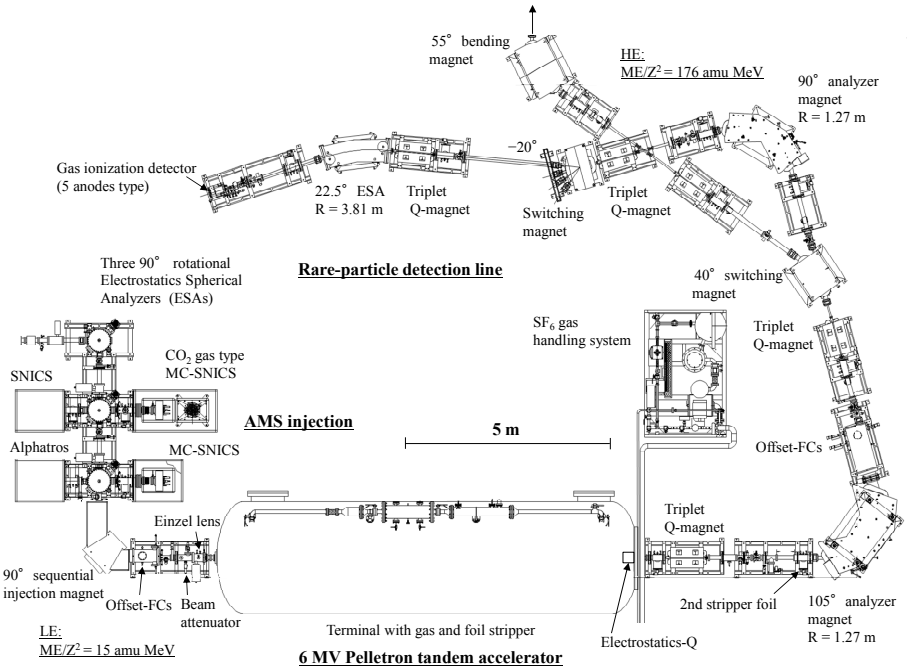

Fig. 1. Details of the Tsukuba 6 MV AMS system.

The Tsukuba 6 MV AMS system is expected to measure all standard AMS species routinely. We simulated AMS performance by using the Particle and Heavy Ion Transport Code System (PHITS) [4]. Fig.

2 shows sample two-dimensional spectra of ^{36}Cl in the gas ionization detector simulated by PHITS. The simulation showed that $^{36}Cl^{7+}$ with an energy of 46.8 MeV is injected into the gas ionization detector. If the entrance window of the gas ionization detector is 150-nm-thick Si_3N_4 foil, the optimal propane gas pressure is estimated to be 42 Torr. The simulation uses ^{36}Cl : ^{36}S = 10,000 : 10,000,000 as the incident particles in the gas ionization detector. The ^{36}Cl was clearly separated from the ^{36}S in the gas ionization detector by the Tsukuba 6 MV AMS system. Table 1 lists the AMS performance of the 6 MV Tsukuba system estimated from PHITS simulations and primary beam tests. The new system will start routine multi-nuclide AMS measurements of ^{10}Be, ^{14}C, ^{26}Al, ^{36}Cl, ^{41}Ca, and ^{129}I in 2015.

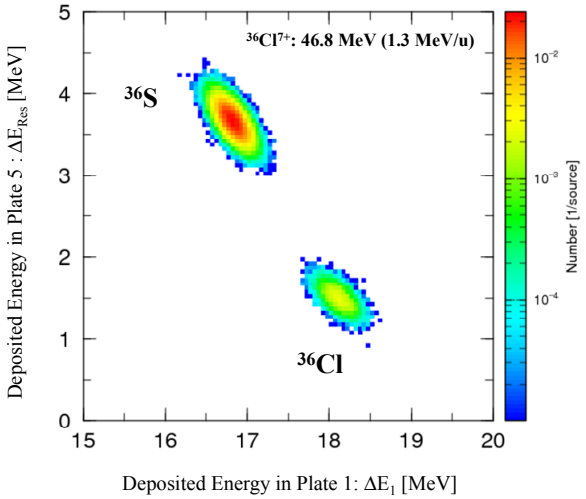

Fig. 2. Two-dimensional spectra of ^{36}Cl AMS in the rare-particle detection system simulated by the PHITS. Partial energy loss in the first anode along the ion path is indicated on the horizontal axis (ΔE_1), and a total residual energy signal from the fifth electrode, a cathode, is shown on the vertical axis (ΔE_{Res}).

Table 1 AMS performance estimated from PHITS simulations and primary beam tests.

Isotopes	**^{10}Be**	**^{14}C**	**^{26}Al**	**^{36}Cl**	**^{41}Ca**	**^{129}I**
Target	BeO	Graphite	Al_2O_3	AgCl	CaF_2	AgI
Injected ion	BeO^-	C^-	Al^-	Cl^-	CaF_3^-	I^-
Injectable ion current (μA)	4	50	1	30	0.3	20
Detected ion/stripper	$^{10}Be^{3+}$ (Gas)	$^{14}C^{4+}$ (Gas)	$^{26}Al^{3+}$ (Gas)	$^{36}Cl^{7+}$ (Foil)	$^{41}Ca^{5+}$ (Gas)	$^{129}I^{4+}$ (Gas)
Terminal voltage (MV)	4.5	4.5	4.3	6	5	3.5
Transmission (%)	20	55	20	20	5	8
Background	2×10^{-15}	5×10^{-16}	5×10^{-15}	1×10^{-15}	3×10^{-14}	1×10^{-14}
Precision (%)	3	0.3	3	3	3	3

References

[1] K. Sasa et al., Nucl. Instr. Meth. B (2015) in press. doi:10.1016/j.nimb.2015.04.028.

[2] S. Xu et al., Radiocarbon 46 (2004) 59–64.

[3] C. Maden et al., Nucl. Instr. Meth. B 259 (2007) 131–139.

[4] T. Sato et al., J. Nucl. Sci. Technol. 50 (2013) 913–923.

1.3 Reconstruction of the Lamb-shift polarized ion source

T. Moriguchi, Y. Yamato, Y. Tagishi, T. Takahashi, S. Ishii, Y. Tajima, D. Sekiba, A. Ozawa

A polarized ion beam is an effective tool for measuring physical quantities such as analyzing power and nuclear magnetic moment. The Lamb-shift polarized ion source (PIS) was installed at UTTAC in 1976 for experimental nuclear physics [1]. The PIS of this type makes it possible to produce highly polarized negative proton and deuteron beams. The PIS, which was located at the 9th floor of the main building, was used as one of the ion sources for the 12UD Pelletron tandem accelerator. However, the PIS was damaged seriously by the Great East Japan Earthquake on 11 March 2011. A part of the damage of the PIS is reported in Ref. [2].

After the disaster, the reconstruction of the PIS was decided to use as the ion source for the newly designed 6 MV tandem accelerator. The new building for the PIS was constructed at the west-side of the accelerator room [3]. Since main components of the PIS such as a duoplasmatron chamber, a spin filter, an argon gas cell, an electrostatic steerer and a Wien filter were reusable, they were moved from the 9th floor of the main building to the new one, and then were reconstructed. Other components and parts of the PIS except for the reusable ones were basically replaced to new ones. Until March 2015, almost all of the reconstruction of the PIS has been completed, as shown in Fig. 1. Fig. 2 shows the present layout of the PIS. New scroll pumps and turbo molecular pumps (magnetic floating type) are used as the present vacuum system. With this vacuum system, the beam line of the PIS is maintained at a vacuum of ~ 10^{-8} Torr. Acceleration tubes, quadrupole magnets and some beam ducts were newly produced and were installed as the beam transport line of the PIS. Gate valves broken by the earthquake were overhauled for reusing. Many new power supplies for operating the PIS are placed on the high voltage insulation stage. This stage was designed originally for the PIS. Most devices on this stage are controlled through optical fibers. For instance, the FAst Spin State Interchange Control System (FASSICS), which was designed newly, is connected to the PIS through optical fibers. This device makes it possible not only to switch a spin state, but also to decide whether or not a beam is polarized. As shown in Fig. 2, a beam produced by the PIS is bent 90° by an electrostatic analyzer (ESA) and transported to the accelerator room through outside of the building.

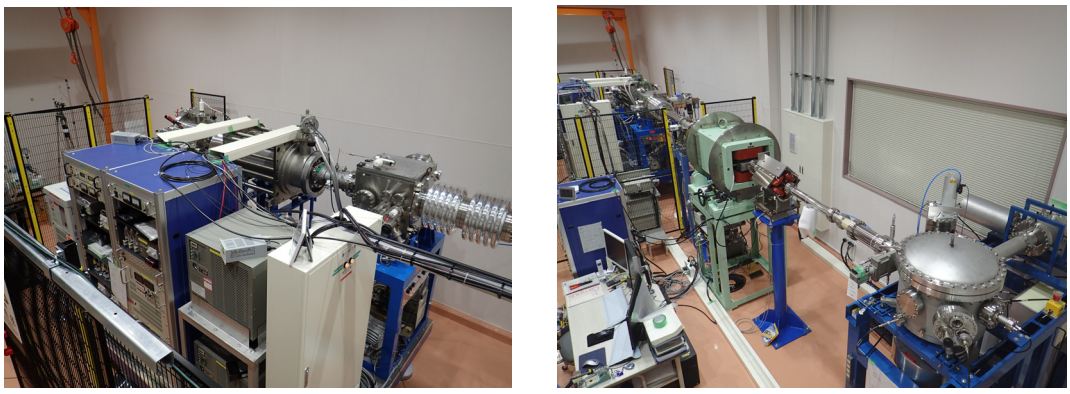

Fig. 1. Pictures of the PIS after the reconstruction.

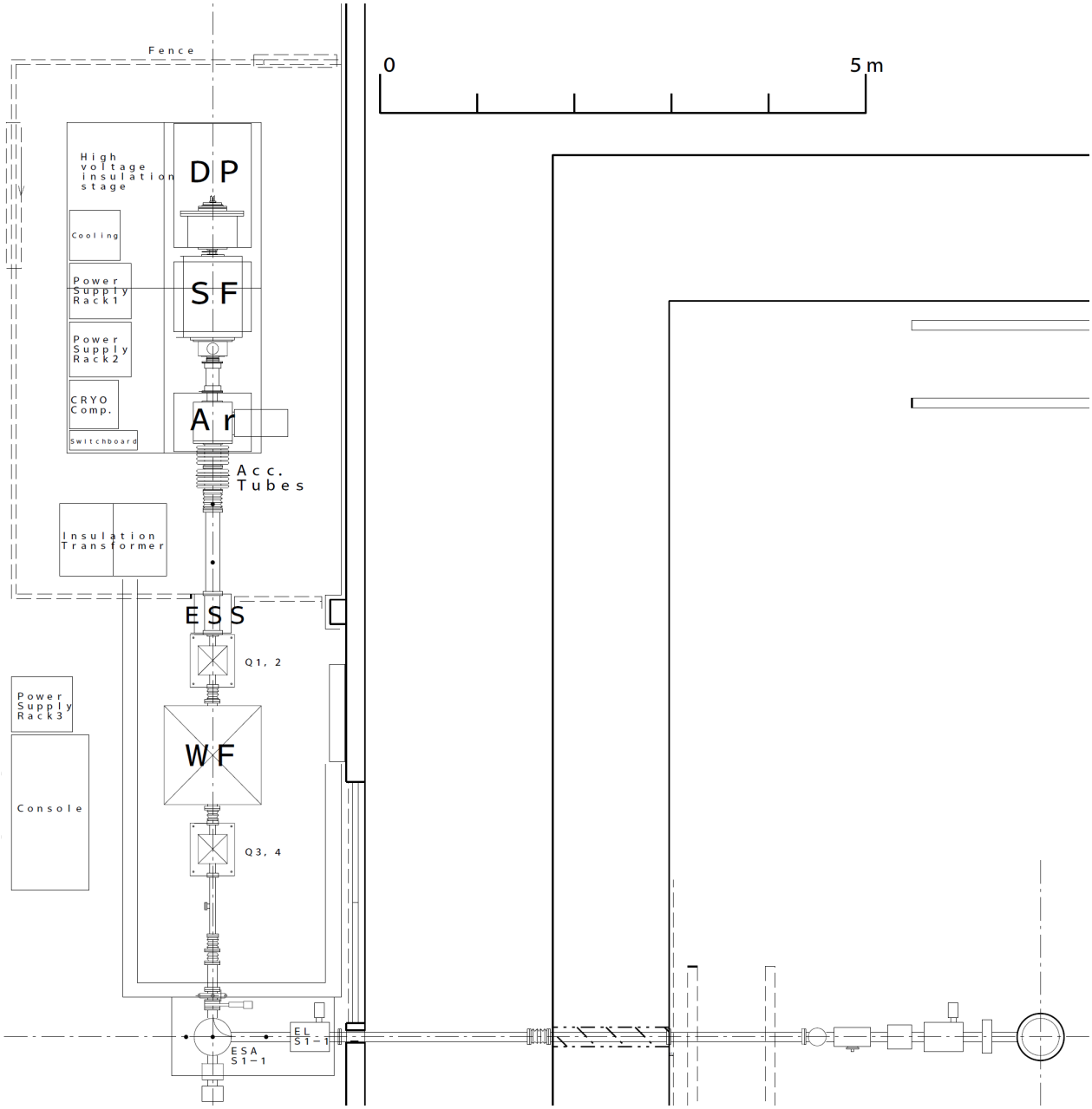

Fig. 2. Present layout of the PIS. The PIS is mainly composed of a duoplasmatron (DP), a spin filter (SF), an argon gas cell (Ar), an electrostatic steerer (ESS) and a Wien filter (WF). A beam produced by the PIS is transported to the accelerator room (the right-hand side) through outside of the building.

We are presently preparing the control system using EPICS for the PIS. After that, we will perform beam tests (intensity, polarization, transmission and so on), and then measure magnetic moment of unstable nuclei with a polarized beam produced by the PIS.

References

[1] Y. Tagishi et al., UTTAC Annual Report 1976 (1977) 12.

[2] K. Sasa et al., UTTAC Annual Report 2010 (2011) 1.

[3] K. Sasa et al., UTTAC Annual Report 2012 (2013) 3.

2.1 Measurements of nuclear moments for unstable nuclei at RCNP

Y. Ishibashi, D. Nagae, Y. Abe, Y. Ichikawa, T. Moriguchi, A. Ozawa, K. Sawahata, H. Ueno[1]

The β-ray detected nuclear magnetic resonance (β-NMR) method [1] is an efficient method to measure the nuclear magnetic (μ) moment of unstable nuclei. The absolute values of μ moments are measured for various nuclei by β-NMR. However, the signs of μ moments are rarely measured experimentally. Therefore, to determine the sign of μ moment, applying a rotating RF is necessary. The rotating RF system has been developped [2,3] to determine the sign of μ moment by β-NMR. In the past, the rotating magnetic field was obtained using two Helmholtz-like coils with axes crossed at right angles, and the experimental apparatus is shown in Reference [3]. In the present work, the rotating magnetic field was controlled by changing the internal phase of a function generator (see Fig. 1) without cable delay. Thereby, without changing the resonance condition of the tank circuit, it was possible to change the phase.

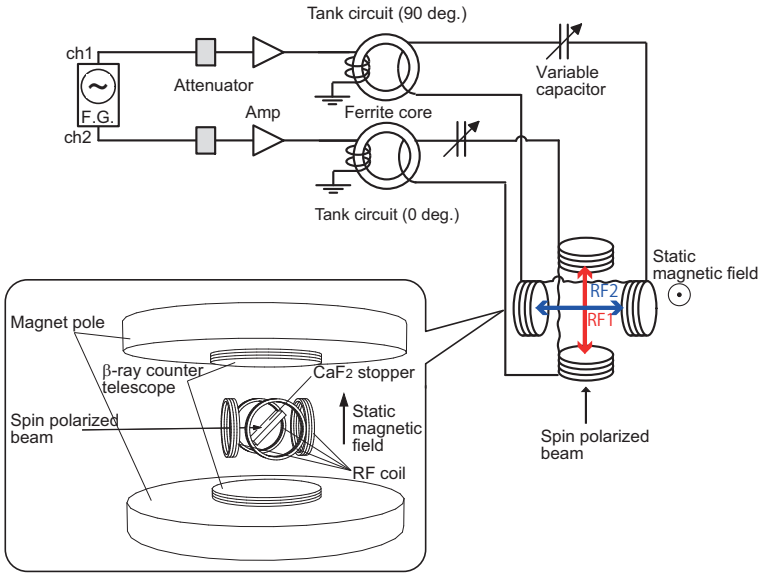

Fig. 1. Block diagram of the RF system for rotating magnetic field and a schematic layout of the β-NMR setup.

In this work, a performance of the system was studied with spin-polarized ^{20}F ($I^{\pi} = 2^{+}$, $T_{1/2}$ = 11.163 s, $\mu(^{20}\mathrm{F})$ = +2.09335(9) μ_N) nuclei at the Research Center for Nuclear Physics, Osaka University. A spin-polarized ^{20}F was produced in the ^{19}F($\vec{d}$, p)^{20}F reaction. In this reaction the polarization of the beam particles is transferred to each nucleus. The $\vec{d}$ beam was produced by a polarized ion source [4], and was accelerated up to E/A = 5 MeV by the AVF cyclotron. The polarized beam was impinged on a CaF_2 crystal (12 mm $\times$ 12 mm $\times$ 1 mm^t) to produce the polarized ^{20}F. The crystal was placed at the center of the β-NMR apparatus, at room temperature with a static magnetic field $B_0 = 350$ mT applied.

The β-rays emitted from ^{20}F nuclei were detected with three plastic scintillator telescopes located above and below the crystal. The up/down ratio R of the β-ray counts is written as $R_0 \approx a(1+A_\beta P)/(1-A_\beta P)$, where a denotes a constant factor representing asymmetries in the counter solid angles and efficien-

[1]RIKEN Nishina Center

cies, A_β and P denote the β-ray asymmetry parameter and the degree of spin-polarization. A rotating RF perpendicular to the B_0 is applied to ^{20}F by using the two pairs of coils. If the frequency and the direction of the rotating RF correspond to the resonant one, the direction of the spin-polarization is inverted ($P \to -P$) by the NMR. Thus, the up/down ratio is changed as $R \approx a(1 - A_\beta P)/(1 + A_\beta P)$. When the polarization is altered due to the resonant spin change, a change appears in the ratio R_0/R. The β-ray asymmetry $A_\beta P$ is written by, $A_\beta P = (\sqrt{(R_0/R)} - 1)/(\sqrt{(R_0/R)} + 1)$.

Typical time spectrum for the β-rays is shown in Fig. 2. The obtained purity of ^{20}F was nearly 100%. In this experiment, we firstly measured μ moment by β-NMR applying the linear RF using tank circuit (0 deg.). Then, we measured the μ moment using a tank circuit (90 deg). The obtained μ moments were consistent with reported values [5]. Finally, we tried to measure the sign of $\mu(^{20}\mathrm{F})$, applying rotating RF. Analysis of the results is in progress.

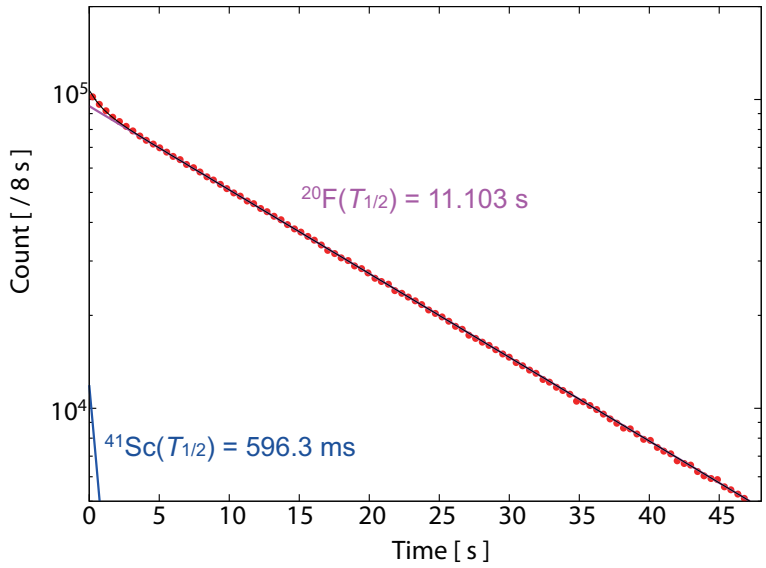

Fig. 2. Typical time spectrum of ^{20}F.

References

[1] K. Sugimoto, et al., J. Phys. Soc. Jpn. 21 (1966) 213.

[2] T. Niwa et al., UTTAC 81 (2012) 5.

[3] D. Nagae et al., Hype. Int., 220 (2013) 65.

[4] K. Hatanaka et al., Nucl. Instr. Meth., 217 (1983) 397.

[5] N.J. Stone, At. Data Nucl. Data Tables 90 (2005) 75.

2.2 Beam irradiation test of Havar foil and Pt target for KISS experiment

M. Mukai, Y. Hirayama[1], N. Ishiyama[1], S.C. Jeong[1], H. Miyatake[1], M. Oyaizu[1], Y.X. Watanabe[1], A. Ozawa

KEK RNB group has developed KEK Isotope Separation System (KISS) [1] to measure the neutron-rich short-lived nuclei related to the astronucleosynthesis. In the KISS project, the gas cell filled with argon gas of 50 kPa is used to stop the target like fragments produced by multi-nucleon transfer reaction of ^{198}Pt target (6 mg/cm^2 in thickness) and $^{136}Xe^{19+}$ beam (E/A = 10.75 MeV, beam size 10 mm in diameter). Extraction efficiency of KISS has achieved about 0.15% with ^{124}Xe beam of 10 pnA so far. To perform the lifetime measurement of ^{200}W with such extraction efficiency, the beam of 100 pnA is required. Such a high beam current may damage the Havar foil (gas cell window) and the ^{198}Pt target. We need to study the limitation of beam intensity as the foils are not broken. We performed beam irradiation test of the Havar foil (3.6 μm in thickness) and the platinum target (1.2 μm in thickness) using $^1H^+$ beam of 1.92 MeV from 1 MV tandetron. Beam current was from 20 pnA to 2 pμA and beam spot size was 2 mm in diameter. Energy losses [W/m^2] of the proton beam in the tested Havar and platinum foils correspond to those of the $^{136}Xe^{19+}$ beam intensities of from 1 pnA to 100 pnA in the Havar foil (3.6 μm in thickness) and from 0.49 pnA to 49 pnA in the ^{198}Pt target (6 mg/cm^2 in thickness).

Experiment was performed using the C-course chamber. To monitor the change of the target thickness, energy of back scattered proton was measured using SSD. SSD was masked with an aperture of 1 mm in diameter and placed at 15 cm away from the target surface and at the angle of about 160 degree from the beam axis. Temperature of target was measured using a radiation thermometer.

Beam irradiation time was one hour with maximum beam current of 1.9 pμA and 2 pμA for the Havar foil and the platinum foil, respectively. Width of the energy distribution of the back scattered proton (Fig. 1) was not changed during the experiment in both targets. It means that target thickness of both targets was not changed. Red gleam from the target surface was observed when the proton beam with the current of higher than 1 pμA was irradiated to both targets. Target temperature of 1223 K in the Havar foil and less than 973 K in the platinum target were measured with maximum beam current. In the Havar foil, a burn mark was observed over the beam spot. However, these

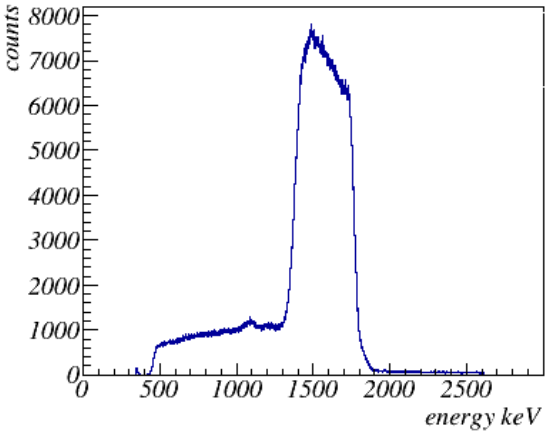

Fig. 1. Measured energy distribution of the back scattered proton from the Havar foil with beam current of 1.9 pμA. Energy distribution below 1300 keV originated from the back scattered protons around a beam duct downstream of the target and a beam collimator upstream the target.

[1] Institute of Particle and Nuclear Studies, High Energy Accelerator Research Organization (KEK), Tsukuba, Ibaraki 305-0801, Japan

measured temperatures are several hundred kelvin lower than the melting points of both materials. It implies that Xe beam with 100 pnA can be available at the KISS on-line experiment.

References

[1] S.C. Jeong et al., KEK Report 2010-2(2010).

2.3 Production of unstable nuclei via resonant proton-capture reactions

A. Ozawa, Y. Ichikawa, T. Moriguchi, K. Sawahata

The proton-capture reactions have been investigated for long time for various stable nuclei and by the various energy range. The motivations for the investigation are based on astrophysical interests and search for excited states of produced nuclei. Among the proton-capture reactions, resonant proton-capture reactions are very interesting since the reaction rate is very large and the reaction occurs even in low energy ($E_p < 500$ keV). Since the energy widths of resonant proton-capture reactions are very narrow, they are also applied to calibrate 'absolute' acceleration energy in accelerators. In the point of production of unstable nuclei, the resonant proton-capture reactions are attractive. In the UTTAC, there is Lamb-shift type polarized ion source, where polarized proton beams are available. If the polarized proton beams are captured, reaction products will be highly polarized. If the products are unstable nuclei, we may obtain highly polarized unstable nuclei. If we obtain the polarized unstable nuclei, we may be able to measure nuclear moments for these nuclei by using β-NMR method.

Among the resonant proton-capture reactions, specially, following reactions are interesting:

^{24}Mg(p,γ)^{25}Al(I=5/2$^+$, $T_{1/2}$=7.1 s) E_p=419 keV E_γ=2.674 MeV

^{29}Si(p,γ)^{30}P(I=1$^+$, $T_{1/2}$=150 s) E_p=417 keV E_γ=5.9 MeV

^{40}Ca(p,γ)^{41}Sc(I=7/2$^+$, $T_{1/2}$=0.6 s) E_p=1842 keV E_γ=2.883 MeV

^{58}Ni(p,γ)^{59}Cu(I=3/2$^-$, $T_{1/2}$=82 s) E_p=1424 keV E_γ=4.82/4.33 MeV

In this list, typical proton-energies for each resonant proton-capture reactions and typical γ-ray energies to be observed in the reactions with the respective proton energies are also shown. All reaction products in the reactions are short-lived unstable nuclei. In the point of nuclear moment measurements, the magnetic moment of ^{30}P is not known. The magnetic moment of ^{59}Cu has a large error bar. The quadrupole moments of ^{25}Al, ^{30}P and ^{59}Cu are not known. Thus, if we obtain large production yields for these nuclei by the resonant proton-capture reactions, investigation of the moments for these nuclei may be possible.

We performed a preliminary experiment to produce ^{25}Al and ^{30}P by the resonant proton-capture reactions in UTTAC. The resonant proton-capture reactions for ^{25}Al and ^{30}P are well investigated [1, 2]. Purposes of the preliminary experiment were to check effective yields and contaminants. We used proton beams with E_p=500 keV accelerated in 1 MV tandem accelerator. We used MgF_2 and MgO target for ^{25}Al production, and Si and SiO_2 targets for ^{30}P production. Thickness of the targets was 0.5 mm. A typical proton-beam intensity was 10 nA. γ-rays from reaction products were measured by a HP-Ge detector. Finally, we irradiated for about 3000 seconds to MgO and Si targets, however we did not observe prominent γ-ray peaks related to ^{25}Al and ^{30}P. We will suppress background events and increase beam intensity in the further measurements and also we will try the production of ^{41}Sc and ^{59}Cu.

References

[1] D.C. Powell et al., Nucl. Phys. A 660 (1999) 349 and references therein.

[2] J.P.L. Reinecke et al., Nucl. Phys. A 435 (1985) 333 and references therein.

3.

ACCELERATOR MASS SPECTROMETRY

3.1 Performance test of automated sample preparation system for ^{14}C-AMS using IAEA reference materials

T. Matsunaka, K. Sasa, K. Sueki, T. Takahashi, M. Matsumura, H. Matsuzaki[1], T. Nakamura[2]

New ^{14}C-AMS system using automated sample preparation system with an elemental analyzer (EA) and CO_2 gas ion source was installed at the University of Tsukuba Tandem Accelerator Complex (UTTAC). Technical innovation of ^{14}C-AMS system is expected in terms of speed-up, high repeatability, low background, and microscale radiocarbon analysis. Firstly, we tested the ability of the sample preparation system using reference materials, which shows known ^{14}C activities from 0 to 150 pMC (percent Modern Carbon), purchased from International Atomic Energy Agency (IAEA) and National Institute of Standards and Technology (NIST).

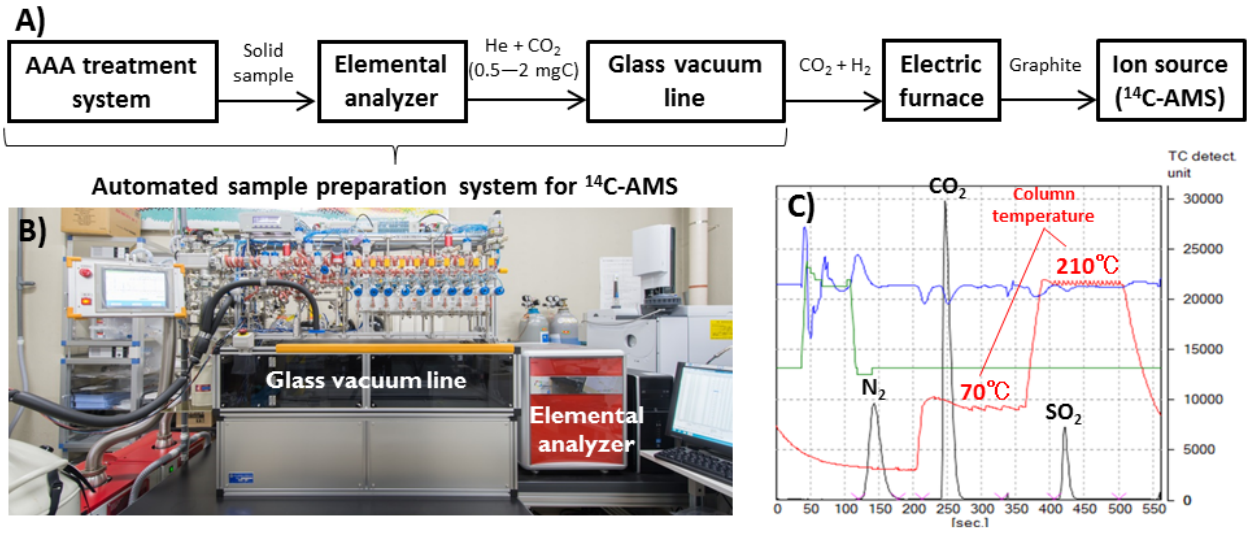

Fig. 1. (A) Conceptual diagram of ^{14}C-AMS system using automated sample preparation system. (B) Photograph of automated class vacuum line coupled with an EA. (C) Chromatogram of N_2, CO_2, and SO_2 separated by the EA.

Graphite materials were prepared using the automated sample preparation system with 20-reactor graphite lines (Fig. 1) from IAEA-C1 (Marble), C2 (Travertine), C3 (Cellulose), C4 (Wood), C5 (Wood), C6 (Sucrose), C7 (Oxalic acid), C8 (Oxalic acid), C9 (Wood), and NIST-4990C (Oxalic acid). Three carbon isotopes of ^{12}C, ^{13}C, and ^{14}C were measured for the graphite with AMS system at Nagoya University and the University of Tokyo. Fig. 2 shows an excellent linear relationship between the wide range of measured and consensus ^{14}C values (pMC) for the reference materials. These measured values are in good agreement with the consensus values. The ^{14}C activities of IAEA-C1 graphite were 0.04 – 0.1 pMC which corresponds to 55,000 – 64,200 yr BP (before present) at late three times, relatively lower than the background level of 0.1 – 0.2 pMC in common laboratories (Fig. 3). Therefore, the automated system is available for ^{14}C dating of old sample until 55,000 yr BP.

[1] The University Museum, The University of Tokyo
[2] Center for Chronological Research, Nagoya University

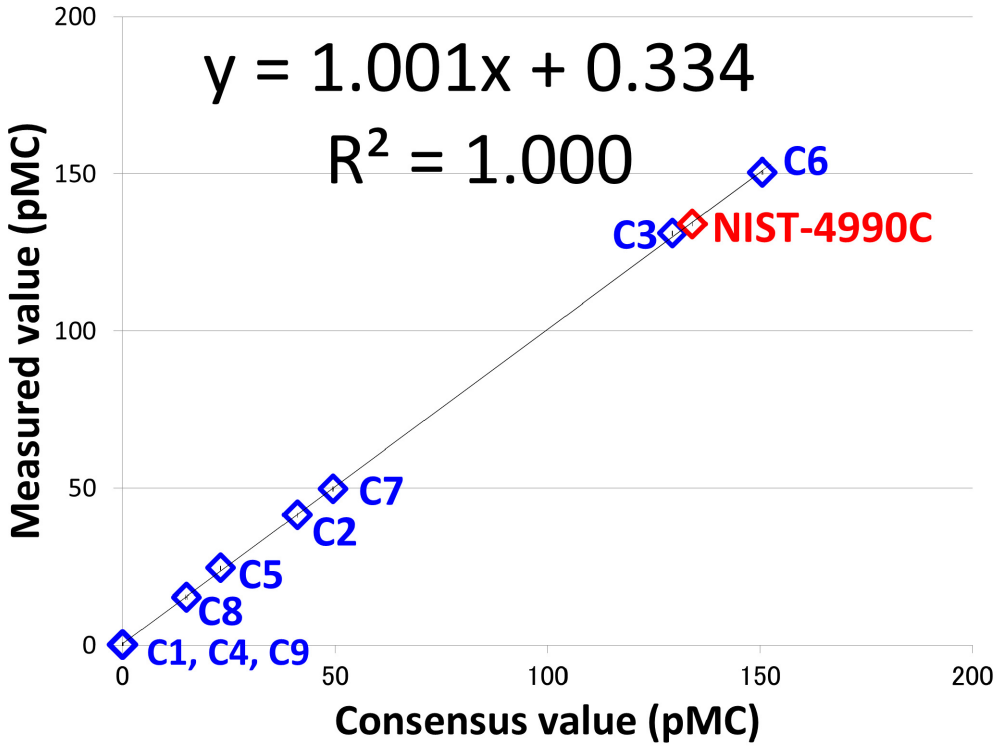

Fig. 2. The correlation between consensus and measured ^{14}C activities of reference materials purchased from IAEA and NIST. The regression line and correlation coefficient (R^2) are shown in the correlation diagram.

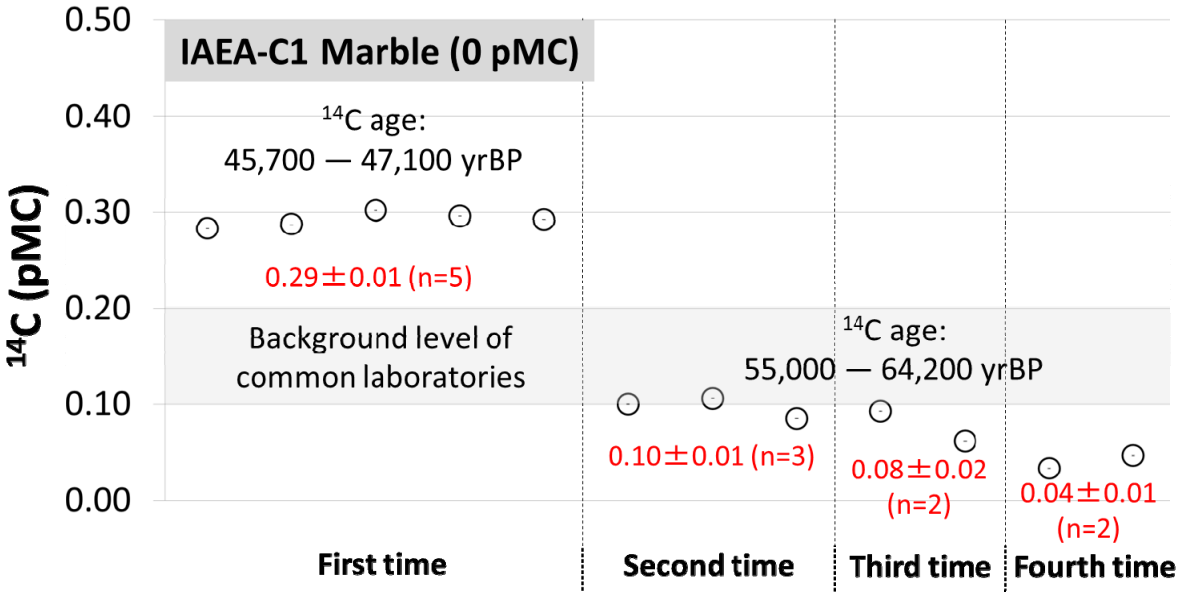

Fig. 3. ^{14}C activities of IAEA-C1 graphite prepared with automated sample preparation system at the University of Tsukuba. Back ground levels of the system are shown from ^{14}C activities and calculated ^{14}C ages of IAEA-C1.

3.2 Study on the migration behavior of Fukushima accident-derived iodine-129 from land area to the marine environment

T. Matsunaka, K. Sasa, K. Sueki, Y. Onda[1], T. Ishimaru[2], K. Taniguchi[1,3], Y. Wakiyama[1,4], M. Honda, T. Takahashi, M. Matsumura, H. Matsuzaki[5]

The March 2011 accident at the Fukushima Dai-ichi Nuclear Power Plant (FDNPP) in Japan results in the massive release of high volatility fission products, including ^{129}I (8.1 GBq [1]) and ^{131}I (120–160 PBq, [2–3]). The long-lived ^{129}I ($T_{1/2}$ = 15.7 million years) is one of the important radionuclides, which we need to evaluate its migration behavior from Japan's land area to the marine environment because of its relatively high chemical reactivity, biological concentration in the marine ecosystem, and affinity for the thyroid gland although it is less radiologically harmful than the short-lived ^{131}I ($T_{1/2}$ = 8.02 days). The present study aimed to evaluate the following three points: 1) the source and the discharge of particulate ^{129}I in the Niida River, 2) ^{129}I distribution in the marine sediment around estuary of the Niida River system, and 3) ^{129}I distribution in the sea water and the marine organism in area close to the FDNPP.

In the Niida River system where the upstream are in the relatively high-contaminated area located 30–40 km northwest from the FDNPP, total suspended solid (SS) each month from December 2012 to January 2014 were continuously collected at Haramachi site (5.5 km upstream from the river mouth) of the downstream river by installing the time-integrative SS sampler. Marin surface sediments (0–3 cm depth) were collected at the two sites within 2 km from mouth of the Niida River. On the other hand, sea water samples of 2 L in water depths of 0 m, 5 m, 10 m, 15 m, and 20 m, and rock fish were collected at a site 6 km south-southeast of the FDNPP in July 2014. The iodine in SS, sediment, and rock fish of 0.2–0.5 g was volatilized and trapped in an organic alkaline solution (~10 ml) by pyrohydrolysis method [4]. After adding 2 mg iodine carrier to the trap solution and the filtered water sample of 1 L, the iodine was isolated and precipitated as AgI. The ^{129}I/^{127}I ratio of AgI targets were measured using an AMS system at the Micro Analysis Laboratory Tandem accelerator (MALT), The University of Tokyo (Matsuzaki et al., 2007). ^{127}I in the trap solution and the water sample were measured by an ICP-MS at the University of Tsukuba. The original ^{129}I activities and ^{129}I/^{127}I ratios in the samples were calculated using ^{127}I concentration obtained from ICP-MS and ^{129}I/^{127}I ratio obtained from AMS.

^{129}I activities and ^{129}I/^{127}I ratios in SS of the Niida River were 0.9–4.1 mBq kg^{-1} and (2.5–4.4)×10^{-8}, which were strongly correlated with the total dry weight of monthly SS samples with correlation coefficient (R^2) of over 0.79. ^{129}I activities and ^{129}I/^{127}I ratios in SS were considered to infer the source of SS (relatively high-level contaminated upstream area or low-level contaminated downstream area). Meanwhile, the discharged particulate ^{129}I at Haramachi site were estimated to be 7.7–12 kBq month^{-1} from September to October 2013. Therefore, relatively massive amount of particulate ^{129}I from the

[1] Center for Research in Isotope and Environmental Dynamics, University of Tsukuba
[2] Oceanographic Observation Center, Tokyo University of Marine Science and Technology
[3] Prefectural centre for Environmental Creation, Fukushima Prefectural Government
[4] Institute of Environmental Radioactivity, Fukushima University
[5] The University Museum, The University of Tokyo

upstream were transported to the downstream of the Niida River from September to October 2013. ^{129}I activities in the surface marine sediments from two sites within 2 km from mouth of the Niida River were 5.8–8.4 μBq kg^{-1}, 2–3 orders of magnitude lower than that of SS at Haramachi site of the Niida River.

The ^{129}I activity in surface sea water collected 40 months after the accident was 2.2 μBq L^{-1} (Fig. 1), ~2 times larger than the previous ^{129}I data in surface sea water collected 3 months after the accident [1]. ^{129}I activities in the rock fish were 42–48 μBq kg^{-1}, approximately 20–400 times larger than that of sea water of same site. There is a possibility of biological ^{129}I concentration in the rock fish. Further investigations are needed to evaluate the mechanism.

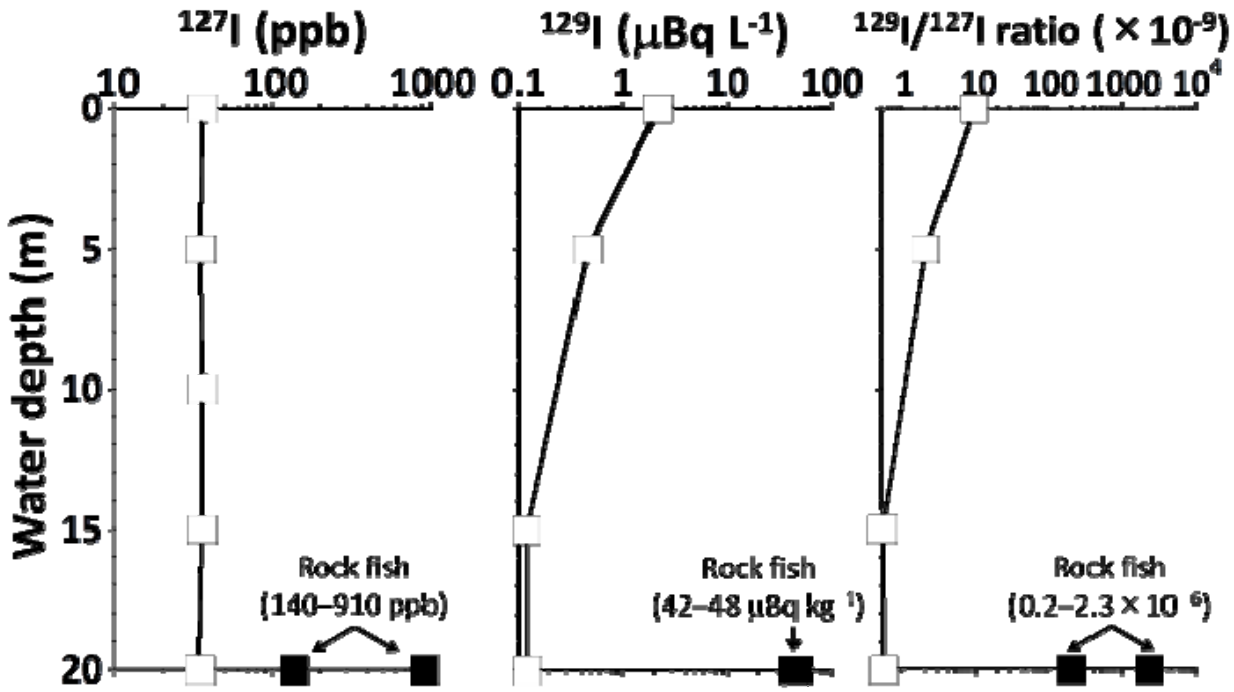

Fig. 1. Profiles of ^{127}I concentration, ^{129}I activity, and ^{129}I/^{127}I ratio in sea water (white squares) and rock fish (black squares) collected at a site 6 km south-southeast of the FDNPP.

References

[1] X.L. Hou, P.P. Povinec, L.Y. Zhang, K. Shi, D. Bidduiph, C.C. Chang, Y. Fan, R. Golser, Y. Hou, M. Jeskovsky, A.J.T. Hull, Q. Liu, M. Lou, P. Steier, W. Zhou, Environ. Sci. Technol. 47 (2013) 3091–3098.

[2] M. Chino, H. Nakayama, H. Nagai, H. Terada, G. Katata, H. Yamazawa, J. Nucl. Sci. Technol. 48 (2011) 1129–1134.

[3] H. Terada, G. Katata, M. Chino, H. Naga, J. Environ, Radioact. 112 (2012) 141–154.

[4] Y. Muramatsu, Y. Takada, H. Matsuzaki, S. Yoshida, Quat. Geochro. 3 (2008) 291–297.

[5] H. Matsuzaki, Y. Muramatsu, K. Kato, M. Yasumoto, C. Nakano, Nucl. Instr. Meth. B 259 (2007) 721–726.

3.3 Changes in $^{129}I/^{127}I$ ratio of crater lake and volcanic activity at Zao volcano

T. Matsunaka, K. Sasa, K. Sueki, T. Takahashi, M. Matsumura, A. Goto[1], T. Watanabe[2], N. Tsuchiya[2], N. Hirano[2] , H. Matsuzaki[3]

The volcanic activity has become higher at Zao volcano in Miyagi and Yamagata Prefectures, Japan, since January 2013 after the 2011 Tohoku Earthquake [1]. Up to 106 times of the monthly volcanic earthquakes were observed in August 2014, and twice of the white turbidity were found in the surface of crater lake in October 2014. Basic water quality of crater lake have been studied by Tohoku University since the water quality of crater lake are correlating with volcanic activity. As a part of this investigation, we are trying to monitor the volcanic activity using $^{129}I/^{127}I$ ratios at Zao volcano.

Long-lived ^{129}I ($T_{1/2}$ = 15.7 million years) is produced in nature by cosmic-ray-induced spallation of xenon in the atmosphere and spontaneous fission of uranium in the lithosphere [2]. Values of $^{129}I/^{127}I$ ratios found nowadays in different environments are 2–8 orders of magnitude larger than that in the pre-nuclear era (1.5×10^{-12}, [3]) by the release of anthropogenic ^{129}I originating from spent nuclear fuel reprocessing, nuclear weapons testing, and nuclear accident [2]. $^{129}I/^{127}I$ ratio in precipitation at Fukushima area rose to $\sim10^{-5}$ soon after the nuclear accident [4]. In our previous study, $^{129}I/^{127}I$ ratio in lake water collected in October 2013 from the crater lake at Zao volcano were 2.2×10^{-9}, which were affected by anthropogenic ^{129}I. In terms of the global iodine cycle, chronologically-old iodine with low isotopic ratio was considered to be supplied into the crater lake from underground corresponding to the volcanic activity, resulting the decrease in $^{129}I/^{127}I$ ratio of the crater lake. The present study aimed to elucidate distribution of $^{129}I/^{127}I$ ratio and source of iodine in the crater lake, and the relativity between $^{129}I/^{127}I$ ratio in the crater lake and volcanic earthquake for the monitoring of volcanic activity at Zao volcano using $^{129}I/^{127}I$ ratio.

Water samples (2 L) were collected 6 times from the surface of crater lake in eastern side of Zao volcano from October 2013 to October 2014 including before and after the white turbidity phenomena. In May 2014, water samples were also collected from the central lake in water depths of 0 m, 6 m, 12 m, and 18 m at the site of ~20 m water depth, snow ice around the lake, and Zao hot spring. After adding 2 mg iodine carrier to the filtered water sample of 1 L, the iodine was isolated and precipitated as AgI. The $^{129}I/^{127}I$ ratio of AgI target was measured using an AMS system at the Micro Analysis Laboratory Tandem accelerator (MALT), The University of Tokyo. ^{127}I in the water sample was measured by an ICP-MS at the University of Tsukuba. The original $^{129}I/^{127}I$ ratios in the water samples were calculated using ^{127}I concentration obtained from ICP-MS and $^{129}I/^{127}I$ ratio obtained from AMS.

$^{129}I/^{127}I$ ratios of the crater lake were $(0.4–5.6)\times10^{-9}$, 2–3 orders of magnitude larger than that of Zao hot spring ($(3.2–5.7)\times10^{-12}$) which is higher contribution of iodine from the underground, and 1–2 orders of magnitude lower than that of snow ice ($(1.0–1.3)\times10^{-8}$) including the anthropogenic ^{129}I. Relatively

[1] Center for Northeast Asian Studies, Tohoku University
[2] Graduate school of Environmental Studies, Tohoku University
[3] The University Museum, The University of Tokyo

high correlation between $^{129}I/^{127}I$ ratios and $1/^{127}I$ was found in the three types of water ($R^2 = 0.69$, n = 13), and the depth profile of $^{129}I/^{127}I$ ratios in the crater lake decreased with depth. Therefore, it is considered that iodine in the crater lake primarily originates from the meteoric water and the underground, and it is also considered that the $^{129}I/^{127}I$ ratios in the lake were determined by the mixing of both sides.

$^{129}I/^{127}I$ ratios of the crater lake increased from 2.2×10^{-9} to 5.6×10^{-9} during October 2013 to the middle of October 2014, and then abruptly decreased to 4.3×10^{-10} soon after the second white turbidity (Fig. 1). A relatively strong negative correlation was found between the $^{129}I/^{127}I$ ratio and monthly volcanic earthquake ($R^2 = 0.68$, n = 4), and there is a possibility that the $^{129}I/^{127}I$ ratio in the crater lake is related to the volcanic activity at Zao volcano. Further investigations are needed for the monitoring of the volcanic activity.

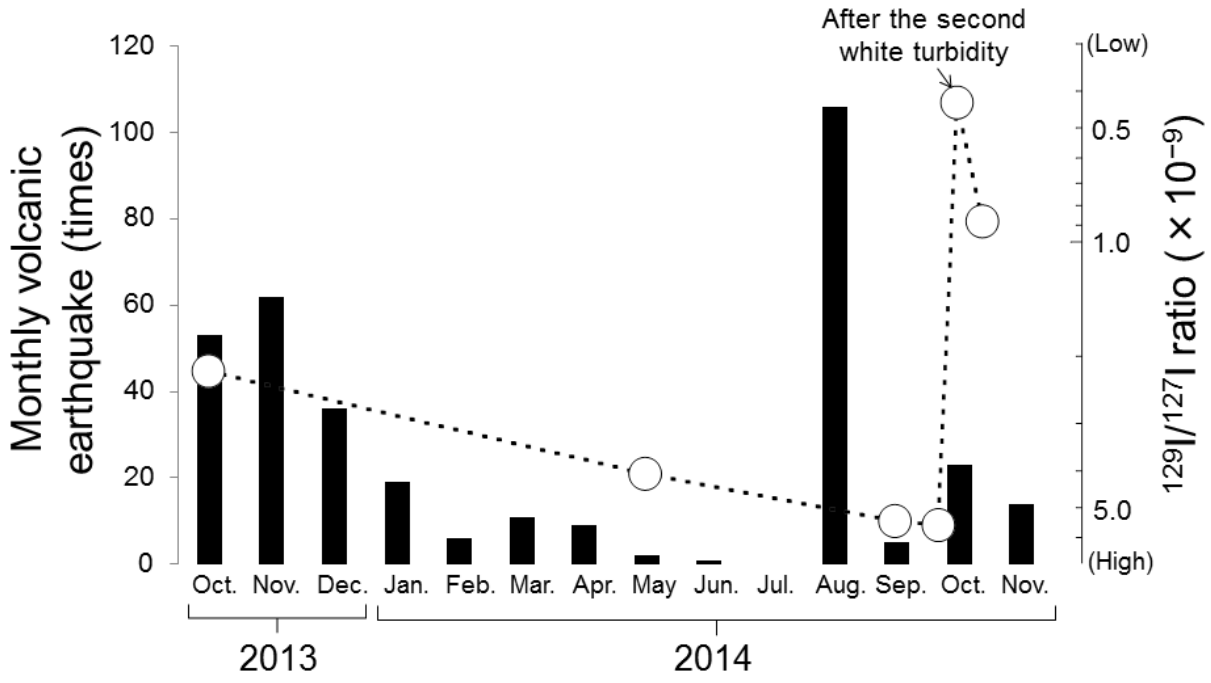

Fig. 1. Temporal changes in $^{129}I/^{127}I$ ratio of crater lake (white circles) and monthly volcanic earthquake (black bar [1]) at Zao volcano.

References

[1] Japan Meteorological Agency Monthly Volcanic Activity Report 2015 (in Japanese).

[2] X.L. Hou, V. Hansen, A. Aldahan, G. Possnert, O.C. Lind, G. Lujaniene, Anal. Chim. Acta, 632 (2009) 181–196.

[3] U. Fehn, J.E. Moran, G.T. Snyder, Y. Muramatsu, Nucl. Instr. Meth. B 259 (2007) 496–502.

[4] S. Xu, S.P.H.T. Freeman, X.L. Hou, A. Watanabe, K. Yamaguchi, L.Y. Zhang, Environ. Sci. Technol. 47 (2013) 10851–10859.

3.4 Technological development for Strontium-90 determination using AMS

Y. Satou, K. Sueki, K. Sasa, T. Matsunaka, T. Takahashi, N. Shibayama[1], D. Izumi, N. Kinoshita[2], H. Matsuzaki[3]

Strontium-90 (^{90}Sr) is a fission product and expected to be released into the environment through such as a nuclear accident. ^{90}Sr quantities are usually measured by chemical isolation of Sr from environmental samples followed by low-level beta counting, however, there are complicated and time-consuming processes to determine ^{90}Sr. Rapid and simple processes are highly required to evaluate ^{90}Sr quantities, especially after the nuclear disaster. The Accelerator Mass Spectrometry (AMS) is one of potential methods which would solve these problems. We have attempted to develop the ^{90}Sr-AMS using the 5 MV tandem accelerator at MALT, the University of Tokyo. We report production tests of negative ion beams and detection tests of ^{90}Zr with the AMS techniques for effective ^{90}Sr measurements. Target samples of SrF_2 were made with chemical separation from the soil at Fukushima. Mixed samples with the purified SrF_2 and PbF_2 were pressed in the aluminum sample holder and installed in the MC-SNICS ion source. The negative ions of $^{88}SrF_3^-$ with over 500 nA were successfully extracted from the MC-SNICS ion source. Natural isobar of ^{90}Zr interferes with ^{90}Sr detection using an ionization chamber. However, in order to observe the behavior of the ^{90}Sr in gas counter, ^{90}Zr isobar was monitored as ^{90}Sr in this study. After the ions passed through a gas stripper, the ions with 90 for mass number and 6+ for charge state, which are considered to be ^{90}Zr, were transported to an ionization chamber. The ions with 1000 cps for count rate were identified in the two-dimensional spectrum in Fig. 1, which correspond to approximately 3×10^{-8} for atom ratio of ^{90}Zr/^{88}Sr in the Sr beam. Further works would provide a successful isobaric separation.

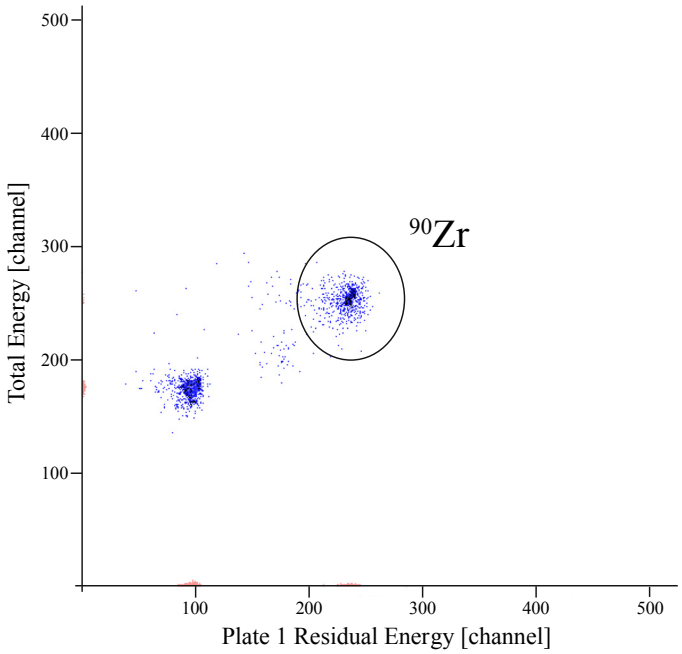

Fig. 1. Spectrum of $^{90}Zr^{6+}$ on gas counter.

[1] University of Tsukuba, Master's Programs of Pure and Applied Science
[2] Institute of Technology, Shimizu Corporation
[3] MALT, The University of Tokyo

3.5 Successive searches of iodine-129 contamination in the chemical sample preparation rooms for AMS

M. Matsumura, K. Sasa, T. Matsunaka, T. Takahashi, Y. Satou, K. Sueki, H. Matsuzaki[1]

Our research involved measuring ^{129}I (half-life: 1.57×10^7 y) in various samples by Accelerator mass spectrometry (AMS) [e.g. 1]. This radionuclide's presence in the atmosphere is attributed to spontaneous fission of uranium, historical nuclear weapon tests, accidents in nuclear facilities, neutron activation analysis, and interactions with cosmic rays. Because halogens such as iodine have volatile species, the rooms used to prepare samples tend to become gradually contaminated through the chemical treatment of samples with high ^{129}I concentrations. AMS can in some cases lead to overestimates of concentrations mainly due to sample contamination, the memory effect and noise at measurement. A sample has a risk to be contaminated during its preparation from its environment and also from other samples. It is important to monitor the contamination in the sample preparation rooms to certify our measurements [2].

Table 1 Details of the rooms measured ^{129}I contamination rates.
Low-level ^{129}I used rooms are located in a building at (A) University of Tsukuba Tandem Accelerator Complex. High-level ^{129}I used rooms are located in a building at (B) the Center for Research in Isotopes andEnvironmental Dynamics, University of Tsukuba.

Research area		History of the room use	Treated samples		
Building name	Room name	Purpose of room use	Kind of sample	Concentration of ^{129}I (atoms g^{-1})	Ratio of ^{129}I/^{127}I
A	C208	Desk work	—	—	—
	C304	Desk work	—	—	—
	C209	Sample preparation	Environmental for ^{36}Cl and final	10^7 to 10^{10}	10^{-11} to 10^{-5}
	C210	Sample preparation	Environmental water	10^7 to 10^{10}	10^{-11} to 10^{-5}
	C108	Sample preparation	Environmental and soil for ^{129}I, enviromental samples for ^{14}C	10^7 to 10^{10}	10^{-11} to 10^{-5}
B	Non-RI room	Sample preparation	Soil	10^9 to 10^{10}	10^{-11} to 10^{-5}
B (Radiation controlled area)	RI room	Sample preparation	Soil etc.	$< 10^{16}$	10^{-4} or more
	ICP-MS room	measurement	Liquid for ICP-MS	$< 10^{13}$	10^{-4} or more
	Passage in front of RI room	Access to RI room	—	—	—

We have started monitoring of ^{129}I from air in our rooms usually used for AMS sample preparations, by a simple method, in a building of University of Tsukuba Tandem Accelerator Complex (UTTAC), Japan, since Aug. 2013 [3]. The ^{129}I monitoring was also performed at rooms known as a high ^{129}I contaminated area in a building of the Center for Research in Isotopes and Environmental Dynamics as well as rooms unrelated with chemistry as background at UTTAC, in order to compare with the results at the sample preparation rooms (table 1). Alkaline trap solutions were placed in the rooms with each three weeks. Stable (^{127}I) and ^{129}I naturally deposited from the atmosphere into the alkaline trap solutions was evaluated. The iodine collection was repeated up to eight times during one year. After three weeks, the amount of the alkaline trap

[1] The University Museum, The University of Tokyo

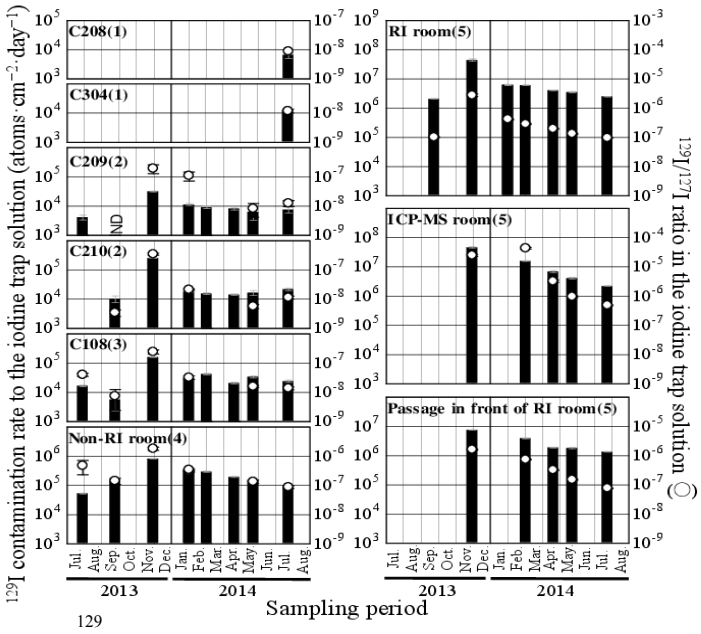

Fig. 1. ^{129}I contamination rate to the iodine trap solution (bar chart) and ^{129}I/^{127}I ratio in the iodine trap solution (white circle).

solutions was obtained through weighing. Then, iodine carrier (with $^{129}I/^{127}I = 1.7 \times 10^{-13}$) was added to the part of trap solutions, the trapped iodine was collected as AgI via chemical purification for AMS. The $^{129}I/^{127}I$ ratio in the trap solutions were determined by AMS at the Micro Analysis Laboratory Tandem accelerator (MALT), the University of Tokyo, Japan [4-5]. Measurement condition was; a terminal voltage was 3.47 MV and charge state was 5+. The measurement results were normalized by Purdue standard material ($^{129}I/^{127}I = 6.54 \times 10^{-11}$): Z94-0596 provided by PRIME Lab., Purdue University [6], the value was revised in 2014 [7]. During all experimental procedures, the blank levels, which included the iodine carrier were $^{129}I/^{127}I = 2.0$ to 5.6×10^{-13}. Also, from the trap solution, approximately 20 mL aliquot was taken for ^{127}I determination by inductively coupled plasma–mass spectrometry (ICP–MS).

Ambient levels of atmospheric ^{129}I in each room were estimated from the measured concentrations in trap solutions as shown Fig. 1. The unit of ^{129}I contamination rate was multiplied by the weight of the original iodine trap solution and by the area of bottle mouth. Strong contamination was consistently observed in all of the rooms during Nov. to Dec. 2013. The increase was attributed to the handling of solutions with high levels of ^{129}I during that time at a certain room. It is concluded that ^{129}I was diffused by air and human movement. Although experimental result was at high risk of overestimation during this period, no sample was prepared fortunately. This raised ^{129}I presence then gradually decreased in all of the rooms. Except for this contamination point, ^{129}I was found to be present at lower than ~10^4 atoms cm^{-2} day^{-1} in the rooms where no-samples and samples with low levels of ^{129}I were handled. Values of 10^4 to 10^5 atoms cm^{-2} day^{-1} were recorded in another room where environmental samples were treated. Higher levels of ^{129}I, ranging from 10^6 to 10^7 atoms cm^{-2} day^{-1}, were recorded in rooms used for treating neutron-activated iodine. With the exception of the values obtained during Nov. to Dec. 2013, the ^{129}I contamination rate and the $^{129}I/^{127}I$ ratio at rooms in UTTAC ranged around 2×10^{-8}, which were also consistent with the ^{129}I level and the $^{129}I/^{127}I$ ratios of environmental level, from atmospheric fallout samples in Tsukuba until 2005 [8].

The experimental results show that the ^{129}I depended on the sample-preparation history of the room. Considering the results of this monitoring, it becomes clear that the sample preparation rooms, in which we actuary used the samples had no serious ^{129}I contamination. This method is valid and simple. We intend to continue the monitoring of ^{129}I from air at sample preparation rooms by this method.

This work was supported by JSPS KAKENHI Grant Numbers 24246156 and 24110006.

References

[1] T. Matsunaka et al., Nucl. Instr. Meth. B, Doi:10.1016/j.nimb.2015.03.056 (available online).

[2] A. Schmidt et al., Sci.Total Environ. 223 (1998)131.

[3] M. Matsumura et al., UTTAC Annual Report 2013 (2014) 31.

[4] H. Matsuzaki et al., Nucl. Instr. Meth. B 259 (2007) 721.

[5] H. Muramatsu et al., Quat.Geochro. 3(2008) 291.

[6] P. Sharma, et al., Nucl. Instr. Meth. B 123 (1997) 347.

[7] M. Caffee, (Purdue University), Personal communication (2014).

[8] C. Toyama, et al., Sci. Technol. 47 (2013) 8383.

4.

BEAM AND ISOTOPE APPLICATIONS

4.1 Micro-PIXE analyses of single fluid inclusions in quartz from Tanzawa granite, Japan

M. Kurosawa, K. Sasa, S. Ishii

Introduction

Fluid released from granitic magma during solidification plays a key role in formation of various metal-ore deposits, hydrothermal alteration, and chemistries of deep groundwater around granite bodies. A part of the fluid is normally trapped as fluid inclusions in the solidified granite and surrounding rocks. Thus, chemical analyses of the inclusions provide useful information about chemistries and behaviors of the fluid. The Miocene plutonic complex in Tanzawa, Kanagawa Prefecture, Japan, is well known for a typical M-type granite [1] and has isotopic and chemical signatures of basaltic rocks derived from the upper mantle [2]. Fluid-inclusion analyses of the Tanzawa granite, therefore, is expected as an information source about chemistries of hydrothermal fluids from M-type granite, because the chemical features have been poorly characterized. For these reasons, we analyzed trace-element contents in fluid inclusions from quartz crystals at the Tanzawa granite by using micro-PIXE.

Sample

The Tanzawa plutonic complex is mainly composed of granite (tonalite) with minor gabbro, and the granite body is subdivided into several rock types. The Yusin type has high SiO_2 contents (>70 wt.%) and demonstrates highly fractionated features [2]. Quartz crystals were collected from miarolitic cavities in the Yusin granite. The quartz included so many two-phase and polyphase inclusions (Fig. 1), minor vapor-rich and liquid-rich inclusions, and trace amounts of liquid-CO_2 inclusion. Elemental compositions of the major two-phase and polyphase inclusions were determined by micro-PIXE. Salinities of the polyphase inclusions were of about 40 wt.% NaCl eq. and the homogenizing temperatures (Th) ranged from 400 to 500 °C. The two-phase inclusions showed almost Th of 220 to 500 °C.

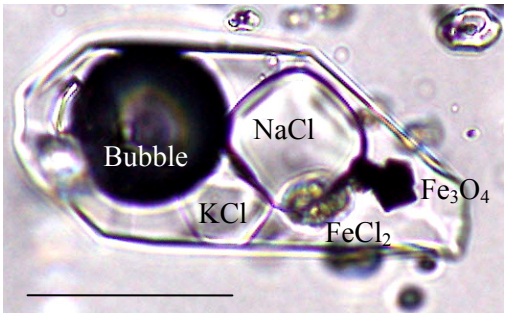

Fig. 1. Photomicrograph of polyphase inclusion in quartz crystal from a miarolitic cavity at the Tanzawa granite, Japan. A large bubble and many daughter crystals of halite, sylvite, and so on are present in the inclusions. Scale bar is a 50 μm.

Experimental

The PIXE analyses were performed at the 1 MV Tandetron. A 0.15 to 0.3 nA beam of 1.92-MeV proton was focused to a 30 × 30 μm spot on the sample using slits and magnetic lenses. The beam incidence was normal to the sample surface, and the X-ray measurement take-off angle was 45° [3,4]. The characteristic X-rays excited by the incident beam were collected by the Si(Li) X-ray-energy detector

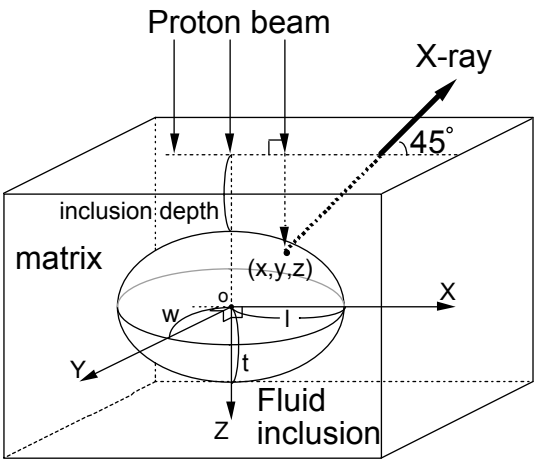

Fig. 2. Schematic geometry for PIXE analysis of fluid inclusion.

(Sirius 30+ detector; e2V Scientific Instruments, UK) with a nominal resolution of 139 eV at 5.9 keV. A 55-μm-thick Mylar film was used to attenuate the intense X-rays from the predominant light elements and to prevent the entry into the detector of protons scattered from samples. The total charge was determined by integrating the target currents, and all samples were analyzed to the integrated charges of 0.4 to 0.9 μC. Analytical points were chosen based on optical viewing using a CCD camera mounted on the microscope [4]. Quantification was performed based on the model of Kurosawa et al. [3,4].

Results and Discussion

PIXE spectrum of a polyphase fluid inclusion in the miarolitic cavities consisted of K X-ray peaks from Cl, K, Ca, Ti, Mn, Fe, Cu, Zn, Br, Rb, and Sr, and of L X-ray peaks from Pb and Ba (Fig. 3). Most of polyphase inclusions in the miarolitic cavities demonstrated the similar X-ray spectra. Element concentrations of the polyphase inclusions, determined by PIXE, were as follows: 20 to 25 wt.% for Cl, 3–8 wt.% for Fe, 3–5 wt.% for K, 0.9–2.7 wt.% for Mn, 1–1.6 wt.% for Ca, 1000–5000 ppm for Zn, about 2200 ppm for Cu, 200–1000 ppm for Pb, 700 ppm for Ba, 270–430 ppm for Br, 30–280 ppm for Ge, 80–200 ppm for Rb, and 0–140 ppm for Sr. The values determined for Cu, Ti, and Mn are several times higher than the values of polyphase inclusions in miarolitic quartz from the Kofu granite, Yamanashi, Japan, which is an I-type Miocene granite [5]. The values for Ge and Sr is extremely lower than those of the Kofu granite. Elemental contents of the two-phase inclusions were as follows: 2.6 to 3.5 wt.% for Cl, 0.2–0.4 wt.% for K, 1000–1900 ppm for Cu, 500–1700 ppm for Fe, 600–1900 ppm for Ca, 700–1700 ppm for Ba, 300 ppm for Mn, 90 ppm for Zn, 15–20 ppm for Br, and 0–30 ppm for Pb and Ge. Rb and Sr contents were undetectable. The extremely lower values of Ge, Rb, Sr, and Pb and the relatively higher contents of Cu, Ti, and Fe are quite different from those of the I-type Kofu granite [5]. The high contents of Cu and Ti and the extremely low contents of Ge and Sr is thought to be a chemical feature of hydrothermal fluids of M-type granite from the comparison to those from the Kofu granite.

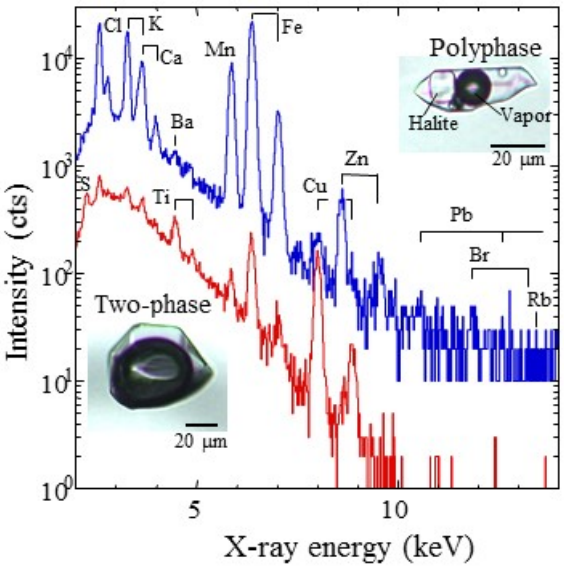

Fig. 3. PIXE spectra of polyphase (upper) and two-phase (lower) fluid inclusions in quartz crystal from miarolitic cavity at the Tanzawa granite, Japan.

The high Cu contents of polyphase and two-phase inclusions are consistent with an existence of sulfide mineral of copper, chalcopyrite, in the miarolitic cavities from the Tanzawa granite. It seems to be metal concentration enough to form large-scale Cu ore deposits near the granite body. The large-scale ore deposits, however, are absent around the granite. This may result from an insufficient total-volume of hydrothermal fluids released from the granite body or lack of concentrated depositions of Cu contents in the fluids at one place. A quick lift-up and erosion of the shallower part around the Tanzawa area associated with the arc–arc collision [2] may be significant for loss of the ore deposits formed often near the earth's surface. An elucidation of the lack of Cu ore deposits at the Tanzawa granite would be important to understanding the cause for absence of a porphyry-Cu type ore-deposits in Japan.

References

[1] M. Takahashi, Modern Geol. 14 (1989) 127.
[2] S. Kawate, M. Arima, Island Arc 7 (1998) 342.
[3] M. Kurosawa et al., Geochim. Cosmochim. Acta 67 (2003) 4337.
[4] M. Kurosawa et al., Nucl. Instr. Meth. B 266 (2008) 3633.
[5] M. Kurosawa et al., Island Arc 19 (2010) 40.

4.2 Coincidence detection system of ion and secondary electron in HERDA

T. Tamura, I. Harayama, S. Maeda, S. Ishii, D. Sekiba

High-resolution Elastic Recoil Detection Analysis (HERDA) equipped with the 90º sector magnet and position sensitive detector (PSD) is an effective tool to determine the hydrogen depth distribution in thin films [1]. While HERDA has an advantage from the viewpoint of the non-destructive method and the ability of quantification, its limit of detection is not enough compared with that of secondary ion mass spectroscopy (SIMS) ~ 10^{18} particles cm^{-3}. The limit of detection in a reasonable data acquisition time directly reflects the ratio between signal and noise. In the case of HERDA, the origins of the noise are attributed to the dark current produced in the micro channel plate (MCP) as the PSD and the stray particles scattered from the inner walls of the vacuum chamber. One of the effective solutions to remove the dark current noise from the data is the coincidence detection of the recoil and secondary electrons emitted from a Mylar film set in front of the PSD. Hashimoto *et al.* applied this coincidence detection system to the High-resolution Rutherford backscattering spectroscopy (HRBS) [2]. The coincidence detection system improved the limit of detection of HRBS for As in Si [3] and that of HERDA for B in Si [4] with the factors of 200 and 20, respectively. In the present study, we tried to determine the limit of detection of HERDA with the coincidence detection system for H in the hydrogenated amorphous carbon (a-C:H) film grown on the Si substrate with chemical vapor deposition (CVD).

Fig. 1. (a) displays the schematics of arrangement of the two PSDs, electrodes to guide the secondary electrons and the stopper foil (Mylar, t = 0.5 μm). Fig. 1. (b), on the other hand, shows a picture of the constructed system. Based on the electrodes arrangement proposed in Ref. [3,4], we simply adopted a flat plate for the electrodes. The blue lines in Fig. 1(a) shows the trajectories of the secondary electrons emitted from the stopper foil put on the PSD1.

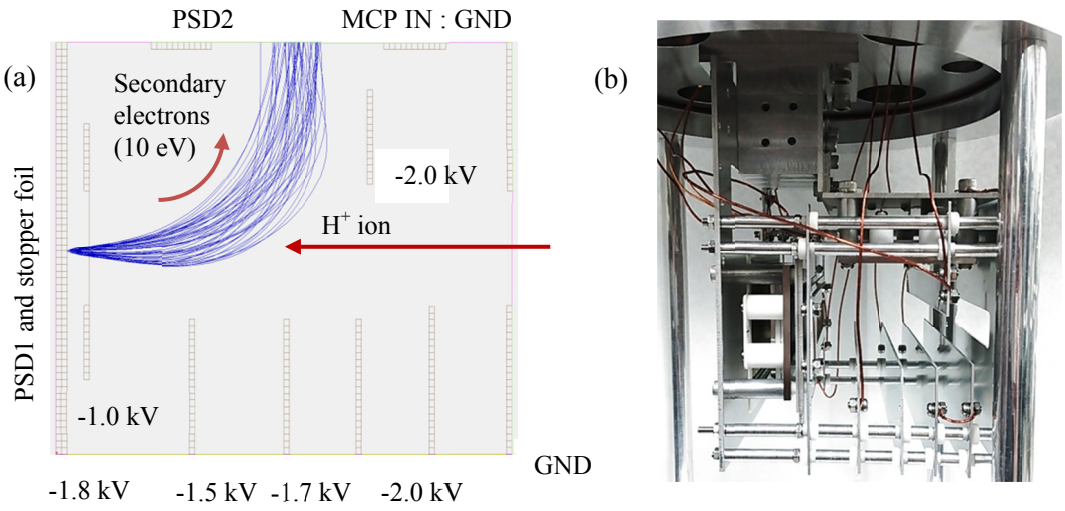

Fig. 1. (a) Schematics electrodes arrangement and electric potentials. (b) A picture of the newly developed coincidence detection system.

The simulation was carried out with a software (SIMION) with an assumption that the initial kinetic energy of the secondary electrons is 10 eV, while this value is not very much sensitive to the trajectory because the secondary electrons immediately accelerated up to ~ 0.8 keV with a Cu mesh toward the PSD2. We can see that the secondary electrons are perfectly collected by PSD2 with the present simple arrangement of electrodes.

Fig. 2 shows the obtained HERDA spectra taken on the a-C:H film with and without the coincidence detection system. In the experiments, 1 MeV $^{16}O+$ was used as the incident beam, and the data acquisition time and irradiation were ~ 300 sec and 5.4 μC, respectively, monitored by a beam chopper. As a result, we observed a remarkable reduction of the dark current noise clearly appeared in the vacuum region of 530 ch ~ 850 ch. The signals of recoils seen in the region of 300 ch ~ 520 ch, however, also showed a significant reduction due to the coincidence detection system. As a total system, the HERDA with the coincidence detection system exhibits the better performance not only for B, but also for H. The problem of the signal loss should be improved in future. In other words, the solution of the signal loss will give us a further major improvement of the limit of detection. The most likely reason of the signal loss seen in the H detection will be a small amount of the emitted secondary electrons induced by the H penetration through the stopper foil. Some coating of the stopper foil to enhance the secondary electron emission might be an efficient improvement in a future work, while some other possible problems, for example, non-suitable setting of time gate generation should be carefully removed.

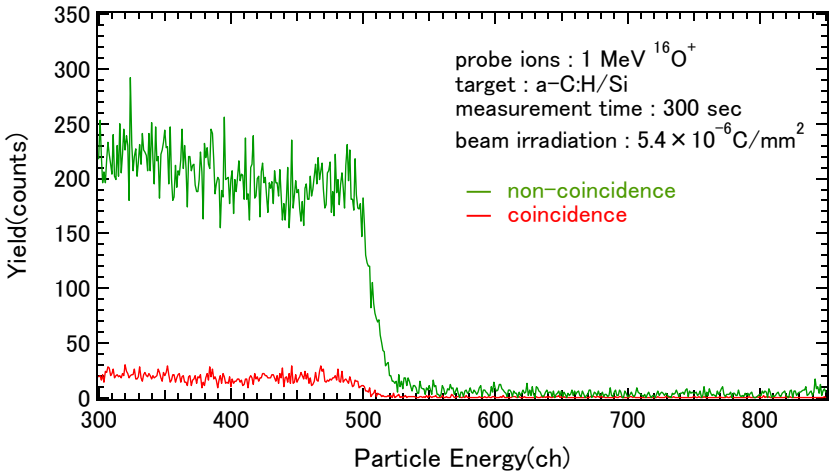

Fig. 2. HERDA spectra taken on the same a-C:H film with (red) and without (green) the coincidence detection system.

References

[1] K. Kimura, K. Nakajima, H. Imura, Nucl. Instr. Meth. B 140 (1998) 397-401.

[2] K. Kimura, M. Mannami, Nucl. Instr. Meth. B 113 (1996) 270-274.

[3] H. Hashimoto, K. Nakajima, M. Suzuki, K. Sasakwa, K. Kimura, Rev. Sci. Instrum. 82 (2011) 063301.

[4] H. Hahimoto, S. Fujita, K. Nakajima, M. Suzuki, K. Sasakawa, K. Kimura, Nucl. Instr. Meth. B 273 (2012) 241-244.

4.3 Straggling effect in channeling on Si(100) with metal thin films

E. Noguchi, D. Sekiba, I. Harayama, Y. Watahiki, S. Ishii

Recently various metal thin films have been grown on substrates by means of chemical vapor deposition (CVD). In contrast to physical vapor deposition (PVD) with the magnetron sputtering, the metal thin films obtained by CVD in principle contain the light elements come from the original process gas, which are usually organic metals. The physical and chemical properties of the metal thin films strongly reflect those contaminations. Therefore the knowledge on the light element distributions are important. When the thickness of an interesting metal film is several nano-meters, high-resolution Rutherford backscattering spectroscopy (HRBS) [1] with channeling is effective to determine the light element distribution in the metal film grown by CVD on a single crystal. In our experience, however, the channeling effect is rapidly suppressed with increasing the film thickness above ~5 nm. To determine the maximum film thickness suitable to the light element distribution analysis by HRBS, we survey the film thickness dependence of yield suppression in channeling on the Pd/Si(100) system.

Five samples were prepared with changing the thickness of the Pd films (t = 4, 8, 9, 13, 14 nm) grown by PVD with the magnetron sputtering on the Si(100) substrate. The dimension of the substrates was 15 mm x 15 mm x 0.5 mm, and the substrate was cleaned fluoric acids before the Pd film deposition. For the channeling measurements, the Si<110> axis was used. The beam incident angle was set at $\theta = 45^{\circ}$ from the surface normal, and then the azimuthal angle ω was swept to observe the channeling dip. HRBS1000 system supplied by KOBELCO with the 1 MV single-end electrostatic accelerator was used. The 400 keV He^{+} beam with a typical current of several tens nA was shaped to 1 mm x 1 mm with a double slit system. The detection angle for the scattered particle was set at 80º with respect to the beam incident direction.

Fig. 1 shows a typical RBS spectrum taken on Pd (t = 8 nm) / Si(100) with the <110> channeling. An intense peak corresponding to the Pd film is seen in the energy region from 360 keV to 380 keV. The signals from the Si substrate are well suppressed due to the channeling, and the leading edge is observed at ~315 keV. The channeling dips depending on the Pd film thickness were plotted by collecting the yield corresponding to the Si subsurface region indicated by the gray hatch (ROI: Region of Interest).

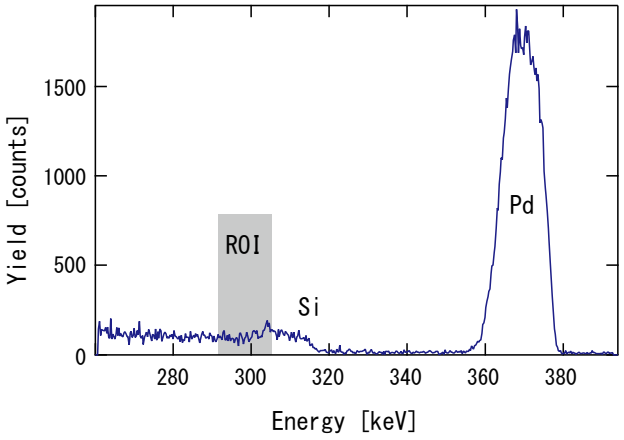

Fig. 1. RBS spectrum taken on Pd (t = 8 nm) / Si(100) with the <110> channeling condition.

Fig. 2(a) shows the channeling dips taken on the five samples around the <110> channeling

with changing the azimuthal angle ω: Pd (t = 4 ~ 24 nm) on Si(100). The yield on the random spectrum Y_{random} is ~800 counts. We can see that the yield at the bottom of the dip Y_{min} increases with increasing the Pd film thickness. Some satellite dips beside the <110> channeling, which correspond to other planar channeling, are also observed when the Pd film thickness is small. Fig. 2(b) displays the minimum yield ratio $\chi_{\mathrm{min}} = Y_{\mathrm{min}} / Y_{\mathrm{random}}$ depending on the Pd film thickness. While χ_{min} = 0.16 was obtained on the Pd (t = 4 nm) /Si(100), the χ_{min} increased up to ~ 0.4 over the film thickness of 10 nm. The value χ_{min} = 0.4 is no longer suitable to the measurements of light element distribution. We tried to interpret the observed behavior of χ_{min} by a theory taking mainly the angular straggling of trajectory to the account [2]. Here primary concept is that the effective critical angle for the channeling $\tilde{\theta}_c$ is reduced from the original value ψ_c by the angular straggling when there is a non-crystalline film on the Si(100) single crystal as follows. $\tilde{\theta}_c = \dfrac{a\,E}{2 Z_{He} Z_{Pd} e^2} \psi_c$. Where "$a$" is the Thomas-Fermi screening radius "E" is the energy of the incident He beam, "e" is the elementary electric charge, Z_{He} and Z_{Pd} are the atomic number of He and Pd, respectively. We can see that the theory well reproduced the present experimental data. From this theoretical model, we survey the experimental condition, which enables us to achieve χ_{min} = ~0.16 with the Pd film thickness of 10 nm. One of the simple solutions is the increase of the He beam energy to suppress the reduction of the effective critical channeling angle. In this case, the He beam energy more than 500 keV is necessary according to the theory. The examination of the beam energy dependence of χ_{min} is remained for the future works.

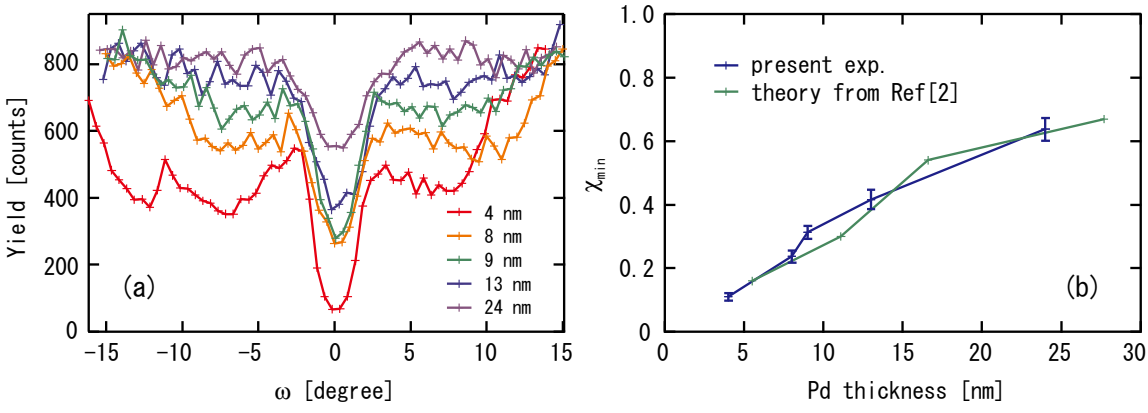

Fig. 2. (a) The channeling dips taken on Pd (t = 4 ~ 24 nm) /Si(100) at the <110> channeling. (b) Pd thickness dependence of minimum yield ratio χ_{min}.

References

[1] K. Kimura, M.Mannami, Nucl. Instr. Meth. B 113 (1996) 270-274.

[2] D.S. Gemmell, Rev. Mod. Phys. 46 (1974) 129-227.

4.4 Mössbauer spectroscopy of ferromagnetic Fe_3O_4 nanoparticles developed for magnetic hyperthermia

H. Latiff, A. Horiuchi, M. Kishimoto, H. Yanagihara, E. Kita

In the application of ferromagnetic nanoparticles to magnetic hyperthermia, coercive force control is an important requirement for effective hysteresis-loss heating within the human-safe limit amplitude H0 and frequency f0 of alternating magnetic field (AMF). Cobalt-contained iron oxide particles were synthesized previously, and the coercive forces was finely tuned according to the Co content. However due to the possible toxicity of cobalt, we attempted to attain coercive force control by introducing the shape anisotropy and synthesized platelet γ-Fe2O3 and Fe3O4 nanoparticles. In this report, platelet Fe3O4 nanoparticles was synthesized and the morphology of particles was investigated using Mössbauer spectroscopy.

Platelet α-FeOOH, used as the precursor materials were synthesized by precipitation and hydrothermal treatment. The α-FeOOH particles were dispersed in tetraethylene glycol (TEG), and heated to the preferred temperature for a certain period of time. TEG is used as the reducing agent in the reaction. The obtained product was washed with ethyl alcohol and then dried in air to powdered form. Magnetizations of dry powdered samples were measured using a vibrating sample magnetometer (VSM) and the variation in crystal structures were examined using X-ray diffraction (XRD). Mössbauer spectroscopy was carried out at room temperature and the velocity and isomer shift were calibrated relative to α-Fe. Data were analyzed using an analysis program, MossWin Ver.4.

Fig. 1 shows the XRD spectra of reduction products heated at 310°C for 5 – 120 minutes. Diffraction peaks attributable to the spinel structure increased with increasing reaction time. After heating for 60 – 120 minutes, single phase spinel structured products were obtained, showing the α-FeOOH particles have completely been reduced to Fe_3O_4.

Fig. 2 shows the room temperature Mössbauer spectra of reduction particles obtained in Fig. 1. Each spectrum was fitted to a combination of two or three magnetic sextets corresponding to Fe oxides and one singlet component. The area ratios of the respective sub-spectra are shown in Fig. 3(a). Fitting parameters are tabulated in Table 1. From the result, it is clear that as the heating time increases, the Fe_3O_4 ratio increases with the expense of α-Fe_2O_3. After 120 minutes, all α-FeOOH have been completely reduced to Fe_3O_4. The singlet component observed in sample heated for 5 minutes, is considered to originate from non-crystalline component which appear during the dehydration process of α-FeOOH. As the reaction time increases, particles grow larger and crystallinity tends to improve thus reducing the singlet component.

Fig. 3(b) shows the magnetic properties of reduction products obtained by heating the α-FeOOH/TEG dispersion at 310°C for 5 – 120 minutes. The saturation magnetization increases rapidly initially and eventually reaches a saturated value. This is due to the rapid formation of magnetic Fe_3O_4 particles in the earlier stage. The coercive forces were almost constant against the reaction time and independent from the saturation magnetization. Although high coercive force has been reported in α-

Fe_2O_3 fine particles, relatively low coercive forces for samples including α- Fe_2O_3 is possibly due to the superparamagnetic relaxation coming from the small particle volumes and magnetic anisotropy. Fe_3O_4 particles obtained after heating for 60 minutes have saturation magnetization of 83 Am^2/kg and coercive force of 13 kA/m. The increase of Fe_3O_4 in expense of α-Fe_2O_3 was also confirmed by Mössbauer spectroscopy analysis shown in Fig. 2 and Fig. 3(a).

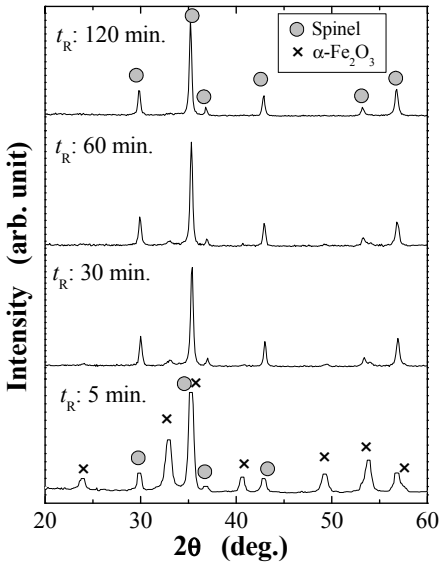

Fig. 1. XRD spectra of the reduction products obtained by heating the α-FeOOH/TEG dispersion at 310°C for 5 – 120 minutes. Dehydration and reduction process of α-FeOOH occurs simultaneously during the first 5 minutes. Reduction process was finally completed after 60 minutes.

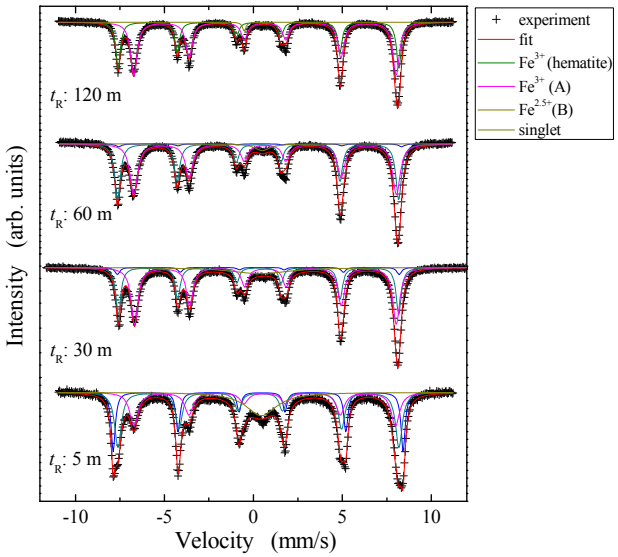

Fig. 2. Mössbauer spectra of samples obtained in Fig. 1 recorded at room temperature. The spectra were fitted to a set of two or three magnetic sextets corresponding to the respective Fe oxides and a singlet component which is considered to originate from non-crystalline component. Reaction times, t_R are 5 – 120 minutes.

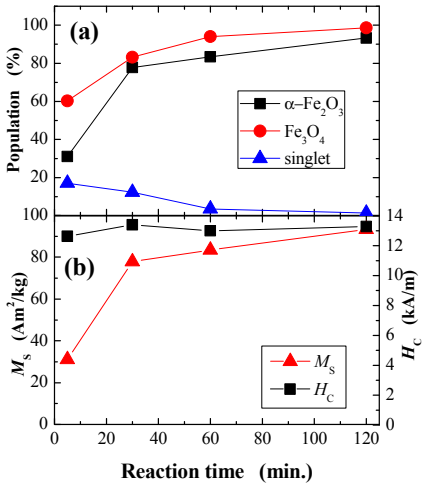

Fig. 3. (a) Population of α-Fe_2O_3, Fe_3O_4, and singlet component deduced from Mössbauer spectra. (b) Saturation magnetizations and coercive forces of reduction products obtained in Fig. 1.

TABLE 1.

MÖSSBAUER PARAMETERS FOR SPECTRA IN

Reaction time (min.)	Ion (site)	H_{hf} (T)	I. S. (mm/s)	Q. S. (mm/s)	Population (%)
5	Fe^{3+}(hematite)	50.6	0.37	-0.21	22.7
	Fe^{3+}(A)	49.1	0.33	-0.10	34.2
	$Fe^{2.5+}$(B)	45.6	0.63	0.00	26.1
	Singlet	-	0.45	-	17.0
30	Fe^{3+}(hematite)	49.2	0.37	-0.20	4.5
	Fe^{3+}(A)	48.9	0.29	-0.02	31.5
	$Fe^{2.5+}$(B)	45.72	0.67	0.00	51.7
	Singlet	-	0.38	-	12.3
60	Fe^{3+}(hematite)	49.5	0.37	-0.12	2.4
	Fe^{3+}(A)	49.1	0.31	-0.02	42.3
	$Fe^{2.5+}$(B)	45.9	0.65	0.00	51.8
	Singlet	-	0.50	-	3.5
120	Fe^{3+}(A)	49.05	0.29	-0.00	37.9
	$Fe^{2.5+}$(B)	45.83	0.65	0.00	60.7
	Singlet	-	-0.52	-	1.4

4.5 Conversion electron Mössbauer spectroscopy (CEMS) of cobalt ferrite thin films

R. Aoyama, H. Yanagihara, K. Mibu[1], E. Kita

High perpendicular magnetic anisotropy (PMA) materials have attracted attention because of their potential use in magnetic recording media and other practical applications. In addition to high PMA, materials that do not contain Pt, a rare metal, are ideal for the future uses to avoid resource issues such as scarcity. The magnetization and PMA of cobalt ferrite thin films, which are high PMA materials, change with composition and production conditions. As such, cobalt ferrite thin films are the subject of our study, and we have reported changes in their magnetization and PMA by changing their composition and production conditions [1].

In order to clarify the mechanism of anisotropy in cobalt ferrite thin films, the electronic and magnetic states should be studied using Mössbauer spectroscopy. However, it is not possible to detect these electronic and magnetic states via transmission through the sample in thin films grown on thick substrates. Conversion electron Mössbauer spectroscopy (CEMS) can be used on such samples because the electrons emitted back from the surface are detected. However, it takes a long time to gather CEMS results from samples thinner than 100 nm because of the insufficient amount of ^{57}Fe nuclei in cobalt ferrite thin films. To decrease measurement time, we prepared a locally enriched ^{57}Fe target [2].

The locally ^{57}Fe enriched target was composed of a 1 mm thick doughnut shaped ^{57}Fe enriched disk, covering the erosion part of sputtering, and a natural Fe base plate. Cobalt ferrite thin films were grown on MgO(001) single crystal substrates by co-sputtering using the locally enriched ^{57}Fe target and Co target. The O_2 flow rate was set to 7 sccm and the substrate temperature was fixed at 600 ºC during sputtering.

Fig. 1 shows a CEMS spectrum for a $Co_{0.65}Fe_{2.35}O_4$ thin film. The time to collect data of equivalent quality was ideally shortened by a factor of ten because the amount of ^{57}Fe was 25% in the enriched target compared to 2.3% in natural Fe. Data collected for 16 hours is shown in Fig. 2, and the spectrum has a distinct enough signal to noise ratio for detailed discussion. The enriched ^{57}Fe combination target enabled us to shorten measuring time drastically and will be a powerful tool in analyzing the magnetic state of Fe based thin films.

The spectrum was fit to a combination of three ferromagnetic sub-spectra, and the result is shown in Fig. 2. The spectrum was fairly symmetric and the isomer shifts were 0.3–0.4 and were fairly similar to those of trivalent Fe ions. It was supposed that about 15% (= $0.35 \cdot 2.35^{-1}$) of Fe atoms were in the divalent state that is not clearly seen in the spectrum. This suggested that the film was well oxidized and the number of divalent Fe atoms was small. Sites with small hyperfine fields (site 1) may be attributed to the surface Fe atoms.

[1] Graduate School of Engineering, Nagoya Institute of Technology, Nagoya 466-8555, Japan

References

[1] T. Niizeki, Y. Utsumi, R. Aoyama, H. Yanagihara, J. Inoue, Y. Yamasaki, H. Nakao, K. Koike, Eiji Kita, Appl. Phys. Lett. 103 (2013) 162407, ibid.104 (2014) 059902 [erratum].

[2] R. Aoyama, H. Yanagihara, Ko Mibu, E. Kita, UTTAC Annual report 2013 (2014) 17.

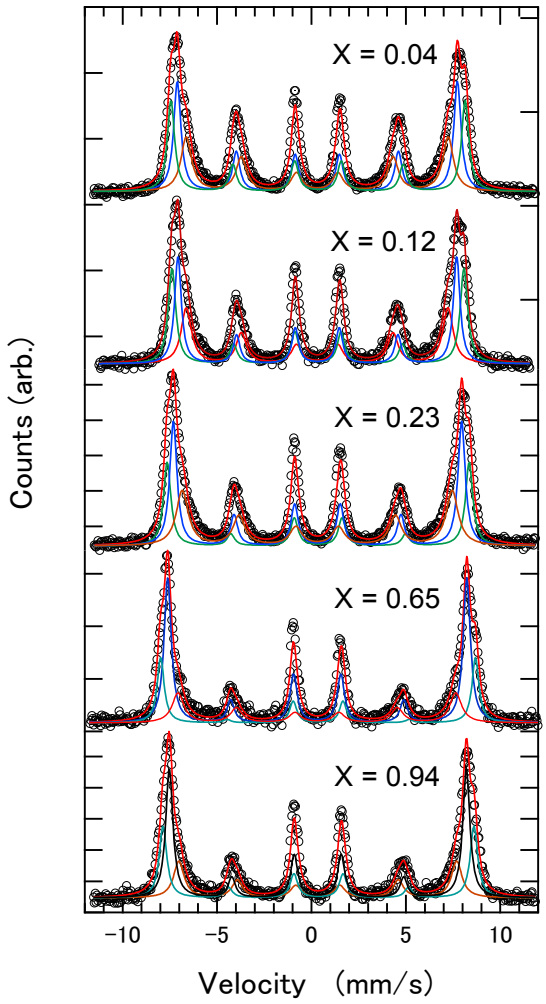

Fig. 1. Conversion electron Mössbauer spectroscopy (CEMS) spectrum for the $Co_xFe_{3-x}O_4$ thin films recorded at 300 K. Solid lines indicate fitted results.

Table 1. Mössbauer fitting parameters for the $Co_xFe_{3-x}O_4$ thin films.

x	H_{hf} (kOe)	*IS (mm/s)	LW (mm/s)	Area (%)	$\overline{H}_{hf}$ (kOe)
0.04	431	0.304	0.682	31.8	
	468	0.311	0.461	37.7	
	484	0.348	0.469	30.5	461
0.12	431	0.300	0.660	32.4	
	459	0.309	0.432	34.8	
	480	0.344	0.480	32.8	457
0.23	444	0.303	0.767	34.9	
	474	0.460	0.319	39.7	
	497	0.355	0.470	25.4	469
0.65	457	0.288	0.745	22.5	
	492	0.307	0.461	55	
	518	0.350	0.450	22.5	490
0.94	457	0.334	0.671	24.3	
	489	0.333	0.456	47.7	
	512	0.372	0.485	28.0	488

*Isomer shift with respect to α-Fe

4.6 Magnetization control of Co ferrite thin films by Kr ion implantation

Y. Liu, E. Kita, H. Yanagihara, K. Mibu[1], D. Oshima[2], T. Kato[3], S. Iwata [2]

According to the increasing demand for high-density recording devices, perpendicular magnetic recording systems have emerged as the predominant hard disk system. For further increase of recording density, stronger perpendicular magnetic anisotropy (PMA) and bit pattern media (BPM) [1] are focused. For BPM, lithography, the imprint technique, or ion implantation have been tested. Ion implantation has been adapted to metallic PMA substances, however, there has been no research on the oxide ferromagnets. Using this technique, one can change/control a magnetic state of materials from ferromagnetic to nonmagnetic, which may render the fill-back process in other lithography techniques unnecessary. We have performed magnetization control by ion implantation on Fe_3O_4 thin films as a basic material of spinel type ferromagnetic oxides.[2,3] Effects of Kr ion implantation was confirmed by Mössbauer study.[3] In this study, a ferromagnetic Co ferrite (CFO) with PMA is focused and the magnetization of them is controlled by Kr ion implantation. We chose the thin films with a concentration of x = 0.75 because the concentration realized high magnetization and PMA.[4]

The thin films of Co ferrite (x=0.75, $Co_xFe_{3-x}O_4$) (13 nm) were grown on polished MgO (001) substrates with a reactive sputtering in an RF planar magnetron sputtering system. In order to perform the Mössbauer spectroscopy measurements, the thin films were fabricated with the Co target and the ^{57}Fe enriched targets.[5] Reflection High Energy Electron Diffraction (RHEED) was used to confirm surface crystalline structure, X-Ray Fluorescence (XRF) was used to analyze the atomic density of Fe and Co atoms, and a SQUID magnetometer was used to measure the magnetization process. Co ferrite thin films were covered with an 15 nm carbon layer prior the ion implantation to prevent a decrease in thickness due to the sputtering by ion beam implantation. Kr ions were accelerated at 30 kV in a conventional ion implantation system.

The influence of Kr ions to the magnetization of Co ferrite thin films was indicated together with that for Fe_3O_4 reported previously[3] in the Fig. 1. The magnetization decreases with the increase of ion dose, and the magnetization of thin films reaches to almost zero when the dose of ions is enough. It is concluded that both thin films are controlled well by Kr ion implantation from these results.

Fig. 2 shows the Mössbauer spectra before and after ion implantation. As-prepared sample shows the spectrum with a distributed hyperfine field. The fitting with three hyperfine fields was carried out. Isomer shifts for subspectra were almost the same magnitude for those of Fe^{3+} ions. After 1×10^{15} ions/cm^2 Kr ions implantation, the ferromagnetic subspectra became small, and the nonmagnetic subspectra became larger. After ion implantation by 1×10^{16} ions/cm^2 Kr ions, the ferromagnetic subspectra shown in the before-ion-implantation sample almost disappeared. It is concluded that the decrease in the magnetization of Co ferrite thin films is due to the Kr ion implantation.

[1] Graduate School of Engineering, Nagoya Institute of Technology, Nagoya, Aichi, Japan.
[2] EcoTopia science Institute, Nagoya University, Nagoya, Aichi, Japan
[3] Department of Electrical Engineering and Computer Science, Nagoya University, Nagoya, Aichi, Japan.

From these, it is considered that the structure of CFO thin film changed partly by the weak Kr ion implantation, and the strain resulting PMA was released. After further implantation, the structure changed into that seen in the Kr irradiated Fe_3O_4 thin films and the magnetization decreased.

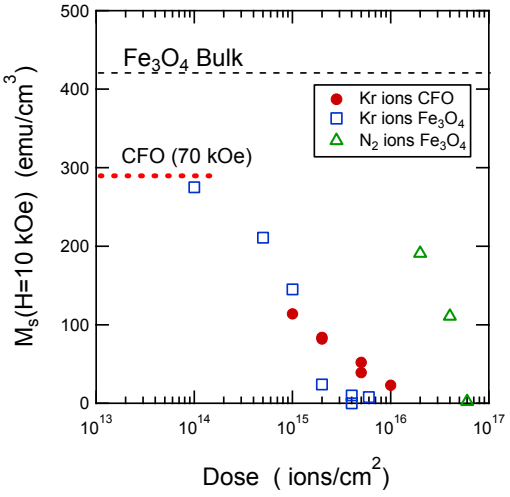

Fig. 1. Influence of Kr ion implantation to magnetization of the Co ferrite thin film and Fe_3O_4 thin films[3].

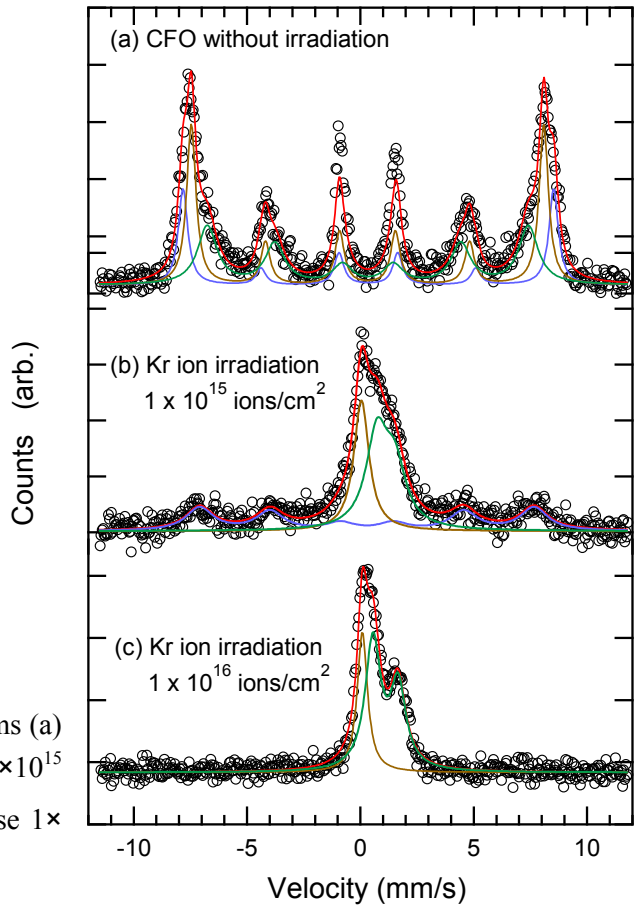

Fig. 2. Mössbauer spectra of Co ferrite thin films (a) without ion implantation, (b) with the dose 1×10^{15} ions/cm^2 ion implantation and (c) with the dose 1×10^{15} ions/cm^2 ion implantation.

Table 1. Mössbauer fitting parameters for a $Co_{0.75}Fe_{2.25}O_4$ thin film without ion implantation.

Sub-spectrum	H_{hf} (T)	IS* (mm·s^{-1})	Line Width(mm·s^{-1})	Area (%)	Estimated site
F1	44.03	0.329	1.034	38.0	B
F2	48.32	0.314	0.496	39.5	A
F3	50.80	0.351	0.501	22.5	B

*Isomer shift with respect to α-Fe

Acknowledgement

Kr ion implantation was performed at Nagoya University with the support of Nanotechnology Platform.

References

[1] B. D. Terris, J. Magn. Magn. Mater. 321 (2009) 512.

[2] E. Kita et al., Jpn. J. Appl. Phys. 53 (2014) 020306.

[3] E. Kita et al., J. Appl. Phys. 115 (2014) 17B907.

[4] T. Niizeki et al., Appl. Phys. Lett. 103 (2013) 162407, ibid. 104 (2014) 059902.

[5] R. Aoyama et al., UTTAC Annual report 2013 (2014) 17.

4.7 Oxygen and sulfur isotopic analysis of ion-induced sulfate production reaction initiated via proton beam

S. Ishino[1], S. Hattori[1], S. Tomita, Y. Nakai[2], N. Yoshida[1]

Ionizing radiation of galactic cosmic ray (GCR) has been recognized as one of the factors influencing the Earth's cloudiness [1]. It has been shown that sulfate is produced and forms small droplets by ionizing radiation [2], but the underlying mechanisms of ion-induced reaction have not yet been identified and their contribution to the atmosphere is still not known.

In order to elucidate the mechanism, we investigated the production of sulfate during ion-induced reaction via proton beam using 1 MV Tandetron accelerator at the University of Tsukuba Tandem Accelerator Complex (UTTAC). The experiments were conducted in two different conditions of the chamber atmosphere; 20 ppm SO_2 mixture in wet air including 20% O_2 (Air mode) and wet N_2 without O_2 (N_2 mode) at relative humidity of 40% and flow rate of 1.0 L min^{-1}. The produced sulfate was collected with PTFE filter (JGWP04700, Merck Millipore) and residual SO_2 was collected by Fe^{2+}/Fe^{3+} solution. Oxygen and sulfur isotope ratios of sulfate and SO_2 were measured using isotope ratio mass spectrometry.

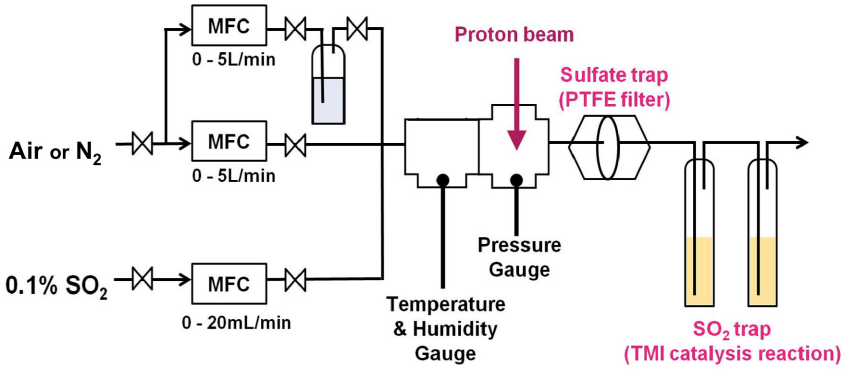

Fig. 1. Experimental setup.

Positive $\Delta^{17}O$ of sulfate was observed in Air mode, while $\Delta^{17}O$ of sulfate in N_2 mode was almost zero. Positive $\Delta^{17}O$ of sulfate in Air mode indicates the contribution of O_3, and these results are consistent with SO_2 oxidation by $O_3^-(H_2O)_x$ clusters, which was predicted through theoretical study [3]. Note that $\Delta^{17}O$ of sulfate in Air mode was smaller than that of atmospheric O_3 suggesting the contribution of other reactions. For N_2 mode, on the other hand, the approximately 0‰ of $\Delta^{17}O$ for sulfate might be due to SO_2 reaction with OH, which was produced by H_2O decomposition promoted by proton beam.[1]

[1] Department of Environmental Chemistry and Engineering and Department of Environmental Science and Technology, Tokyo Institute of Technology, Yokohama 226-8502, Japan
[2] Radioactive Isotope Physics Laboratory, RIKEN Nishina Center, Wako, Saitama 351-0198, Japan

Table 1. $\Delta^{17}O$ values of produced sulfate in this study, sulfate calculated in the model based on *Savarino et al.* [4], and assumptions about the atmospheric oxidants

Sample	Oxidant	$\Delta^{17}O$(oxidant)	$\Delta^{17}O$(sulfate)	References
Air mode	?	–	1.2±0.6	This study
N_2 mode	?	–	–0.7±0.6	
Reference values	OH	0	0	[5]
	O_2	–0.34	–0.09	[6]
	O_3	40	10	based on [7]
	H_2O_2	1.3	0.7	[8]

For the sulfur isotopic compositions ($\delta^{34}S$), there was no significant difference between N2 mode and Air mode. However, the $\delta^{34}S$ values observed in this study were much smaller than that of the major atmospheric sulfate productions in previous study [9, 10].

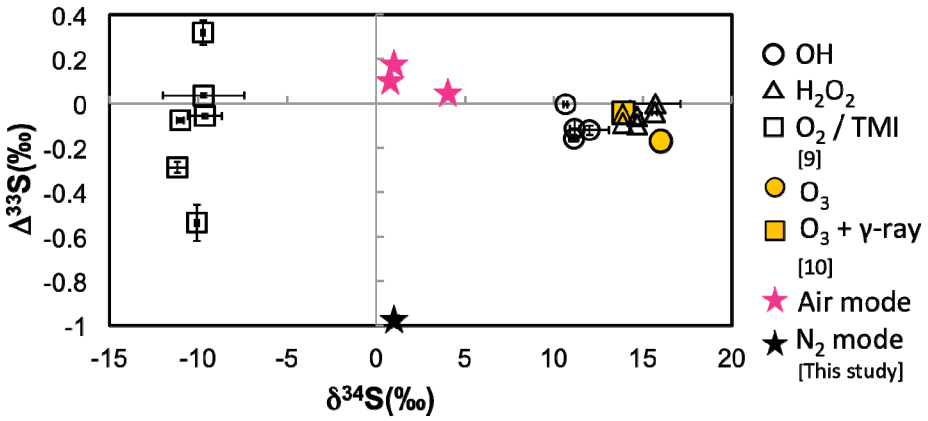

Fig. 2. Comparison of sulfur isotopic fractionation between sulfate production reactions in this study and previous studies.

References

[1] H. Svensmark, E. F. Christensen, J. Atmos. Solar-Terrestrial Phys. 59, 11 (1997) 1225-1232.

[2] H. Svensmark, J. O. P. Pederson, N. D. Marsh, M. B. Enghoff, U. I. Uggerhoj, Proc. R. Soc. A 463 (2007) 385-396.

[3] N. Bork, T. Kurtén, H. Vehkamäki, Atmos. Chem. Phys. 13 (2013) 3695-3703.

[4] J. Savarino, C. C. W. Lee, M. H. Thiemens, J. Geophys. Res. 105, D23 (2000) 29079-29088.

[5] B. D. Holt, R. Kumar, P.T. Cunningham, Atmos. Environ. 15, 4 (1981) 557-566.

[6] E. Barkan, , B. Luz, Rapid Commun. Mass Spectrom. 19 (2005) 3737-3742.

[7] G. Michalski, S. K. Bhattacharya, G. Girsch, Atmos. Chem. Phys. 14 (2014) 4935-4953.

[8] J. Savarino, M. H. Thiemens, J. Phys. Chem. A 103, 46 (1999) 9221-9229.

[9] E. Harris, B. Sinha, P. Hoppe, S. Ono, Environ. Sci. Technol. 47, 21 (2013), 12174-12183.

[10] M. B. Enghoff, N. Bork, S. Hattori, C. Meusinger, M. Nakagawa, J. O. P. Pedersen, S. Danielache, Y. Ueno, M. S. Johnson, N. Yoshida, H. Svensmark, Atmos. Chem. Phys. 12 (2012) 5319-5327.

5.

PUBLICATIONS

5.1 Journals

ACCELERATOR AND EXPERIMENTAL FACILITIES

1. S. Tomita, Y. Shiina, S. Tamura, R. Kinoshita, S. Ishii, K. Sasa, "Measurement of backward secondary-electron yield under molecular ion impact coincident with emerging projectiles", Nucl. Instrum. Meth. Phys. Res. B **354** (2015) 109.

NUCLEAR PHYSICS

2. Y. G. Ma, D. Q. Fang, X. Y. Sun, P. Zhou, Y. Togano, N. Aoi, H. Baba, X. Z. Cai, X. G. Cao, J. G. Chen, Y. Fu, W. Guo, Y. Hara, T. Honda, Z. G. Hu, K. Ieki, Y. Ishibashi, Y. Ito, N. Iwasa, S. Kanno, T. Kawabata, H. Kimura, Y. Kondo, K. Kurita, M. Kurokawa, T. Moriguchi, H. Murakami, H. Ooishi, K. Okada, S. Ota, A. Ozawa, H. Sakurai, S. Shimoura, R. Shioda, E. Takeshita, S. Takeuchi, W. D. Tian, H. W. Wang, J. S. Wang, M. Wang, K. Yamada, Y. Yamada, Y. Yasuda, K. Yoneda, G. Q. Zhang, T. Motobayashi, "Different mechanism of two-proton emission from proton-rich nuclei ^{23}Al and ^{22}Mg", Phys. Lett. B **743** (2015) 306.

3. T. Moriguchi, A. Ozawa, S. Ishimoto, Y. Abe, M. Fukuda, I. Hachiuma, Y. Ishibashi, Y. Ito, T. Kuboki, M. Lantz, D. Nagae, K. Namihira, D. Nishimura, T. Ohtsubo, H. Ooishi, T. Suda, H. Suzuki, T. Suzuki, M. Takechi, K. Tanaka, T. Yamaguchi, "Density distribution of ^{14}Be from reaction cross-section measurements", Nucl. Phys. A **929** (2014) 83.

4. A. Ozawa, T. Moriguchi, T. Ohtsubo, N. Aoi, D. Q. Fang, N. Fukuda, M. Fukuda, H. Geissel, I. Hachiuma, N. Inabe, Y. Ishibashi, S. Ishimoto, Y. Ito, T. Izumikawa, D. Kameda, T. Kubo, T. Kuboki, K. Kusaka, M. Lantz, Y. G. Ma, M. Mihara, Y. Miyashita, S. Momota, D. Nagae, K. Namihira, D. Nishimura, H. Ooishi, Y. Ohkuma, T. Ohnishi, M. Ohtake, K. Ogawa, Y. Shimbara, T. Suda, T. Sumikama, H. Suzuki, S. Suzuki, T. Suzuki, M. Takechi, H. Takeda, K. Tanaka, R. Watanabe, M. Winkler, T. Yamaguchi, Y. Yanagisawa, Y. Yasuda, K. Yoshinaga, A. Yoshida, K. Yoshida, "Charge-changing cross sections of ^{30}Ne, ^{32,33}Na with a proton target", Phys. Rev. C **89** (2014) 044602.

5. T. Komatsubara, S. Kubono, T. Hayakawa, T. Shizuma, A. Ozawa, Y. Ito, Y. Ishibashi, T. Moriguchi, H. Yamaguchi, D. Kahl, S. Hayakawa, Dam Nguyen Binh, A. A. Chen, J. Chen, K. Setoodehnia, and T. Kajino, "Excited states above the proton threshold in ^{26}Si", Eur. Phys. J. A **50** (2014) 136.

6. M. Takechi, S. Suzuki, D. Nishimura, M. Fukuda, T. Ohtsubo, M. Nagashima, T. Suzuki, T.

Yamaguchi, A. Ozawa, T. Moriguchi, H. Ohishi, T. Sumikama, H. Geissel, N. Aoi, Rui-Jiu Chen, De-Qing Fang, N. Fukuda, S. Fukuoka, H. Furuki, N. Inabe, Y. Ishibashi, T. Itoh, T. Izumikawa, D. Kameda, T. Kubo, M. Lantz, C. S. Lee, Yu-Gang Ma, K. Matsuta, M. Mihara, S. Momota, D. Nagae, R. Nishikiori, T. Niwa, T. Ohnishi, K. Okumura, M. Ohtake, T. Ogura, H. Sakurai, K. Sato, Y. Shimbara, H. Suzuki, H. Takeda, S. Takeuchi, K. Tanaka, M. Tanaka, H. Uenishi, M. Winkler, Y. Yanagisawa, S. Watanabe, K. Minomo, S. Tagami, M. Shimada, M. Kimura, T. Matsumoto, Y. R. Shimizu, M. Yahiro, "Evidence of halo structure in ^{37}Mg observed via reaction cross sections and intruder orbitals beyond the island of inversion", Phys. Rev. C **90** (2014) 061305(R).

7. T. Yamaguchi, A. Enomoto, J. Kouno, S. Yamaki, S. Matsunaga, F. Suzaki, T. Suzuki, Y. Abe, D. Nagae, S. Okada, A. Ozawa, Y. Saito, K. Sawahata, A. Kitagawa, S. Sato, "Cherenkov light detection as a velocity selector for uranium fission products at intermediate energies", Nucl. Instrum. Meth. Phys. Res. A **766** (2014) 123.

8. T. Komatsubara, S. Kubono, T. Hayakawa, T. Shizuma, A. Ozawa, Y. Ito, Y. Ishibashi, T. Moriguchi, H. Yamaguchi, D. Kahl, S. Hayakawa, Dam Nguyen Binh, A. A. Chen, J. Chen, K. Setoodehnia, T. Kajino, "Excited states above the proton threshold in ^{26}Si", Euro. Phys. J. A **50** (2014) 136.

9. E. Mcneice, K. Setoodehnia, B. Singh, Y. Abe, D. N. Binh, A. A. Chen, J. Chen, S. Cherubini, S. Fukuoka, T. Hashimoto, T. Hayakawa, Y. Ishibashi, Y. Ito, D. Kahl, T. Komatsubara, S. Kubono, T. Moriguchi, D. Nagae, R. Nishikiori, T. Niwa, A. Ozawa, T. Shizuma, H. Suzuki, H. Yamaguchi, T. Yuasa, "In-beam γ-ray spectroscopy of ^{30}P via the ^{28}Si(^{3}He, pγ)^{30}P reaction", Nucl. Data Sheets **120** (2014) 88.

ACCELERATOR MASS SPECTROMETRY

10. Y. Satou, K. Sueki, K. Sasa, J. Kitagawa, S. Ikarashi, N. Kinoshita, "Vertical distribution and formation analysis of the ^{131}I, ^{137}Cs, ^{129m}Te, and ^{110m}Ag from the Fukushima Dai-ichi Nuclear Power Plant in the beach soil", J. Radioanal. Nucl. Chem. **303(2)** (2015) 1197.

11. T. Matsunaka, K. Sasa, K.Sueki, T. Takahashi, M. Matsumura, Y. Satou, J. Kitagawa, N. Kinoshita, H. Matsuzaki, "Post-accident response of near-surface ^{129}I levels and ^{129}I/^{127}I ratios in areas close to the Fukushima Dai-ichi Nuclear Power Plant, Japan", Nucl. Instrum. Meth. Phys. Res. B, (2015) http://dx.doi.org/10.1016/j.nimb.2015.03.056.

12. D. Oka, Y. Hirose, H. Kamisaka, T. Fukumura, K. Sasa, S. Ishii, H. Matsuzaki, Y. Sato, Y. Ikuhara, T. Hasegawa, "Possible ferroelectricity in perovskite oxynitride $SrTaO_2N$ epitaxial thin films", Scientific Reports **4** (2014) 4987.

13. H. Iida, S. Iguchi, N. Teramoto, K. Koshino, T. Zeniya, A. Yamamoto, N. Kudomi, T. Moriguchi, Y. Hori, J. Enmi, H. Kawashima, N. J. Shah, J. Nakagawara. "Adequacy of a compartment model for $CMRO_2$ quantitation using ^{15}O-labeled oxygen and PET – A clearance measurement of ^{15}O-radioactivity following intra-carotid bolus injection of ^{15}O-labeled oxy-hemoglobin on Macaca fascicularis", Journal of Cerebral Blood Flow & Metabolism **34** (2014) 1434.

14. K. Koshino, K. Fukushima, M. Fukumoto, Y. Hori, T. Moriguchi, T. Zeniya, Y. Nishimura, K. Kiso, H. Iida, "Quantification of myocardial blood flow using ^{201}Tl SPECT and population based input function", Ann. Nucl. Med. **28(9)** (2014) 880.

15. Y. Hori, Y. Hirano, K. Koshino, T. Moriguchi, S. Iguchi, A. Yamamoto, J. Enmi, H. Kawashima, T. Zeniya, N. Morita, J. Nakagawara, M. Casey, H. Iida, "Validity of using a 3-dimensional PET scanner during inhalation of ^{15}O-labeled oxygen for quantitative assessment of regional metabolic rate of oxygen in man", Phys. Med. Biol. **59** (2014) 5593.

16. T. Temma, K. Koshino, T. Moriguchi, J. Enmi, H. Iida, "PET quantification of cerebral oxygen metabolism in small animals", Scientific World Journal, **2014** (2014) 159103.

17. Y. Hata, K. Yamaugchi, K. Kinoshita, E. Kita, T. Mochiku, H. Yasuoka, "Fe ion distribution and superconductivity of $FeSr_2RECu_2O_{6+y}$ (RE = Eu, Er, Gd, Nd and Y)", Physica C **507** (2014) 85.

18. K. Ito, T. Sanai, Y. Yasutomi, T. Gushi, K. Toko, H. Yanagihara, M. Tsunoda, E. Kita, T. Suemasu, "Mössbauer study on epitaxial $Co_xFe_{4-x}N$ films grown by molecular beam epitaxy", J. Appl. Phys. **117** (2015)17B717.

19. K. Kurita, D. Sekiba, I. Harayama, K. Chito, Y. Harada, H. Kiuchi, M. Oshima, S. Takagi, M. Matsuo, R. Sato, K. Aoki, S. Orimo, "Multi-phonon excitations in Fe2p RIXS on Mg_2FeH_6K.", J. Phys. Soc. Jpn. **84** (2015) 043201.

20. K. Ozeki, D. Sekiba, A. Uedono, K. K. Hirakuri, T. Masuzawa, "Effect of incorporation of deuterium on vacancy-type defects of a-C:H films prepared by plasma CVD", Appl. Surf. Sci. **330** (2015) 142.

21. H. Oikawa, R. Akiyama, K. Kanazawa, S. Kuroda, I. Harayama, K. Nagashima, D. Sekiba, Y. Ashizawa, A. Tsukamoto, K. Nakagawa, N. Ota, “Deposition and characterization of amorphous aluminum nitride thin films for a gate insulator”, Thin Solid Films **574** (2015) 110.

22. K. Mase, K. Hiraga, S. Arae, R. Kanemura, Y. Takano, K. Yanase, Y. Ogashiwa, N. Shohata, N. Kanayama, T. Kakiuchi, S. Ohno, D. Sekiba, K. K. Okudaira, M. Okusawa, M. Tanaka, “Decay processes of Si2s core holes in Si(111)-7x7 revealed by Si Auger electron Si2s photoelectron coincidence measurements”, J. Phys. Soc. Jpn. **83** (2014) 094704.

5.2 International conferences

1. M. Ohshima, J. Enmi, M. Tsuji, T. Moriguchi, H. Fukuda, Y. Hashikawa, T. Zeniya, H. Kawashima, K. Koshino, H. Iida, “The hybrid PET and MR imaging of cerebral hemodynamids in rats with hypoxic-ischemic brain injury”, XIII Turku PET Symposium, Turku PET Center, 24-27 May 2014, Finland.

2. J. Enmi, Y. Hashikawa, H. Fukuda, T. Moriguchi, M. Ohshima, K. Koshino, H. Kawashima, T. Zeniya, M. Tsuji, H. Iida, “In vivo imaging-supported development of an intraluminal suture-based technique for acute-to-chronic cerebral infarction model in rat”, World Molecular Imaging Congress (WMIC2014), COEX Convention Center, 17-20 September 2014, Soul, Korea.

3. A. Ozawa, Mass measurement with Rare-RI Ring, Workshop ‘Science and Next Generation Experiments at FRIB and RIBF’ in 4th Joint Meeting of the APS Division of Nuclear Physics and the Physical Society of Japan, 7-11 October 2014, Waikoloa, Hawaii, USA.

4. Y. Abe, Isochronous field study of the Rare-RI Ring, STORI'14 - 9th International Conference on Nuclear Physics at Storage Rings, 28 September - 3 October 2014, Schloss Rheinfels, St. Goar, Germany.

5. H. Tsuchida, K. Nakajima, J. Yokoe, M. Sugiyama, T. Majima, S. Tomita, K. Sasa, Y. Saitoh, K. Narumi, A. Chiba, K. Yamada, S. Matoba, K. Hirata, H. Shibata, K. Kimura, and A. Itoh, “Wake effects on fast-molecular transmission through nanocapillaries”, 26th International Conference on Atomic Collisions in Solids (ICACS-26), 13-18 July 2014, Debrecen, Hungary.

6. Y. Shiina, R. Kinoshita, S. Tamura, K. Sasa, S. Ishii and S. Tomita, “Cluster effect on the yield of secondary electrons produced by single electron excitation”, 26th International Conference on Atomic Collisions in Solids (ICACS-26), 13-18 July 2014. Debrecen, Hungary.

7. Y. Satou, K. Sueki, K. Sasa, T. Matsunaka, N. Shibayama, T. Takahashi N. Kinoshita, “Activity ratios in soil contaminated by the source of different reactor condition in the FDNPP accident”, European Geosciences Union General Assembly 2014, 27 April - 2 May 2014, Vienna, Austria.

8. Y. Onda, K. Sueki, K. Sasa, T. Matsunaka, M. Honda, Y. Wakiyama, V. Golosov, A. Konoplev, K. Namba, T. Takase, “Research project on Niida river basin”, International Symposium on Interdisciplinary Study on Environmental Transfer of Radionuclides from the Fukushima Daiichi NPP Accident, 9-10 January 2015, Tsukuba, Japan.

9. T. Matsunaka, K. Sasa, K. Sueki, T. Takahasi, M. Matsumura, Y. Satou, N. Shibayama, J. Kitagawa, N. Kinoshita, H. Matsuzaki, "Depth profiles of ^{129}I and ^{129}I / ^{127}I ratio in soil at the near-field site of the Fukushima Dai-ichi Nuclear Power Plant", The 13th International Conference on Accelerator Mass Spectrometry, 24-29 August 2014, Provence, France.

10. T. Matsunaka, K.Sasa, K. Sueki, N. Shibayama, T. Takahashi, M. Matsumura, Y. Satou, H. Matsuzaki, A. Goto, T. Watanabe, N. Tsuchiya, N. Hirano, A. Kizaki, "Study on monitoring of volcanic activity using ^{129}I / ^{127}I ratios in crater lake and hot spring at Zao volcano, Japan", The 13th International Conference on Accelerator Mass Spectrometry, 24-29 August 2014, Provence, France.

11. K. Sasa, K. Sueki, T. Takahashi, M. Matsumura, T. Matsunaka, Y. Satou, N. Shibayama, N. Kinoshita, J. Kitagawa, K. Nishihara, H. Matsuzaki, "Distribution of ^{129}I in terrestrial environment released from the Fukushima Dai-ichi Nuclear Power Plant accident", The 13th International Conference on Accelerator Mass Spectrometry, 24-29 August 2014, Provence, France.

12. K. Sueki, N. Shibayama, Y.Satou, K. Sasa, T. Takahashi, T. Matsunaka, M. Matsumura, H. Matsuzaki, M. Murakami, R.Yamashita, S.Mahua, H. Takada, Y. Koibuchi, L. Soulichan, O. Haecong, G. Mouri, T. Oki, "Behavior of Iodine-129 and Radioactive Cesium in Japanese River", The 13th International Conference on Accelerator Mass Spectrometry, 24-29 August 2014, Provence, France.

13. Y. M. Matsumura, N. Shibayama, T. Matsunaka, K. Sasa, K. Sueki, T. Takahashi, Y. Satou, H. Matsuzaki, "Successive comparison of the extent of ^{129}I contamination in the sample preparation room", The 13th International Conference on Accelerator Mass Spectrometry, 24-29 August 2014, Provence, France.

14. Y. Satou, K. Sueki, K. Sasa, T. Matsunaka, , T. Takahashi, N. Shibayama, D. Izumi, N. Kinoshita, H. Matsuzaki, "Development of Strontium-90 AMS in Japan: Progress report", The 13th International Conference on Accelerator Mass Spectrometry, 24-29 August 2014, Provence, France.

15. K. Sasa, T. Takahashi, K. Sueki, T. Matsunaka, M. Matsumura, Y. Satou, D. Izumi, "The new 6MV AMS system at the University of Tsukuba", The 13th International Conference on Accelerator Mass Spectrometry, 24-29 August, 2014, Provence, France.

16. Xiangdong Ruan, Zhaoming Xiong, Kimikazu Sasa, Hongtao Shen, Yongjing Guan, "Radiocarbon Dating of an Ancinent Tomb in Hepu Country, China", The 13th International Conference on Accelerator Mass Spectrometry, 24-29 August 2014, Provence, France.

17. Y.Miyake, H. Matsuzaki, K. Sasa, T. Takahashi, “Measurement of Chlorine-36 in surface soil around F1NPP accident site”, The 13th International Conference on Accelerator Mass Spectrometry, 24-29 August 2014, Provence, France.

18. Y. Satou, K. Sueki, K. Sasa, T. Matsunaka, N. Shibayama, T. Takahashi, N. Kinoshita, “Source estimation of radioactive materials on the ground at the northwestern area from the Fukushima Dai-ichi Nuclear Power Plant”, Asia Oceania Geosciences Society 2014, 28 July - 1 August 2014, Sapporo, Japan.

19. I. Harayama, K. Nagashima, Y. Hirose, H. Oikawa, R. Akiyama, S. Kuroda, H. Matsuzaki, D. Sekiba, “ΔE-E telescope ERDA on AlN films with 40 MeV $^{35}Cl^{7+}$ beam: Development of gas ionization chamber placed on ICF152”, 21st International Conference on Ion Beam Analysis, 23-28 June 2013, Seattle, USA.

20. K. Kurita, D. Sekiba, I. Harayama, K. Chito, Y. Harada, H. Kiuchi, C. Sakai, M. Oshima, K. Sodeyama, Y. Tateyama, R. Sato, M. Matsuo, S. Orimo, “Ultra high resolution Resonant Inelastic soft X-ray Scattering for Mg_2FeH_6”, 8th International Conference on Inelastic X-ray Scattering, SLAC National Accelerator Laboratory Menlo Park, 11-16 August 2013, California, USA.

6.

THESES

Master's theses

Shunnpi AOYAMA	Magnetic properties of $Co_xFe_{3-x}O_4$ (001) thin films prepared by reactive sputtering with dual targets.
Fumiya ARAI	Ion surfing RF-carpet gascell for superheavy element mass measurement.
Daiki IZUMI	Development of AMS measuring condition using the PHITS code and measurement of cosmogenic nuclides.
Akari HORIUCHI	Preparation and magnetic properties of Fe oxides nanoparticles from oval platelet α-FeOOH precursor.
Yang LIU	Magnetization control of Kr ion implantation to $CoFe_2O_4$ thin films.
Kazuki SAWAHATA	Measurement of charge-changing cross-section for proton-rich Si and Ar isotopes.

Undergraduate's theses

Eri NOGUCHI	Straggling effect in channeling on Si(100) with amorphous metal thin films.
Takahiro TAMURA	Coincidence detection system of ion and secondary electron in HERDA.
Ryohei TOMITA	Behavior of dissolved radionuclides and ions in riverine water after FDNPP accident.
Masaya WATANABE	The variation of flux of ^{129}I in Tsukuba region.

7.

SYMPOSIA

The 15th Japanese national workshop on surface and interface ion beam analysis

5-6, December 2014

University of Tsukuba, Tandem Accelerator Complex,

Cooperative Research Building C C305

December, 5 Friday

13:00 - 13:05

Welcome Address

Prof. Eiji Kita

(Research Facility Center for Science and Technology, Univ. of Tsukuba, Vice- Director (TAC section))

Session 1 Chair : Dr. Kenji Kimura

13:05 - 13:45 (Invited talk)

"Investigating surfaces and interfaces with light ions: MEIS and HIM"

Torgny Gustafsson

(Department of Physics and Astronomy, Rutgers University, Piscataway, NJ, USA)

13:45 - 14:15 (Invited talk)

"Helium Ion Microscopy (HIM) for Imaging, Characterization, and nano-Fabrication for nano-Device Materials and Structures"

Shinichi Ogawa

(NeRI, National Institute of Advanced Industrial Science and Technology (AIST))

14:15 - 14:55 (Invited talk)

"Studies on Surface Structure using Fast Atom Diffraction (FAD)"

H. Winter, M. Busch, J. Lienemann, E. Meyer, A. Schüller, J. Seifert

(Institut für Physik, Humboldt-Universität, Berlin, Germany)

Session 2 Chair : Dr. T. Nakamoto

15:10 - 15:35 (Invited talk)

"Ion Beam Guiding with Straight and Curved Insulator Capillaries"

Takao M. Kojima[1], Tokihiro Ikeda[2], Yasuyuki Kanai[1], Vladimir A. Esaulov[3] and Yasunori Yamazaki[1]

([1]Atomic Physics Laboratory, RIKEN, [2]Nishina Center for Accelerator-Based Science, RIKEN, [3]Institut des Sciences Moléculaires d'Orsay, Universite Paris Sud)

15:35 - 15:55

"Formation of SOI structure by ultrahigh-temperature oxygen implantation"

Yasushi Hoshino, Tomohiro Kamikawa, and Jyoji Nakata

(Department of Mathematics and Physics, Kanagawa University)

15:55 - 16:15

"Shape Elongation of Embedded Zn Nanoparticles in SiO_2 by Swift Heavy Ion Irradiation"

H. Amekura[1], D. Tsuya[1], N. Okubo[2], and N. Ishikawa[2]

([1]National Institute for Materials Science (NIMS), [2]Japan Atomic Energy Agency (JAEA))

16:15 - 16:45 (Invited talk)

"Sensitivity Increase with Etched Tracks on a SiO_2 Waveguide in Palmtop Sensor"

Koichi Awazu, Makoto Fujimaki and Xiaomin Wang

(National Institute of Advanced Industrial Science and Technology (AIST))

UTTAC facility introduction and tour

16:55 - 17:20 facility introduction

"Scientific strategy of UTTAC (Univ. of Tsukuba, Tandem Accelerator Complex) with new 6 MV tandem accelerator and high-resolution ion beam analysis"

K. Sasa, T. Moriguchi and D. Sekiba

(UTTAC, Univ. of Tsukuba)

17: 20 - 18:00 facility tour

December, 6 Saturday

Session 3 Chair : Dr. Shigeo Tomita

9:00 - 9:25 (Invited talk)

"Proton Irradiation in Liquid with Glass Capillaries and Metallic Particle Formation by Radiation Reduction"

T.Kobayashi[1], T. Yamaki[2], T. Hakoda[2], S. Yamamoto[2] and Y. Yamazaki[1]

([1]RIKEN, [2]JAEA)

9:25 - 9:45

"Liquid-surface structural analysis by MeV ion microbeams through capillaries"

S. Nomura[1], K. Miyahara[1], R. Furuya[1], J. Wang[1], T. Majima[1,2], M. Imai[2], H. Tsuchida[1,2], and A. Itoh[1,2]

([1]Department of Nuclear Engineering, Kyoto University, [2]Quantum Science and Engineering Center, Kyoto University)

9:45 - 10:05

"Irradiation of liquid droplets with MEV-energy ions in vacuum"

K. Kitajima[1], T. Majima[2], Y. Oonishi[1], H. Ueda[1], H. Tsuchida[2], and A. Itoh[1,2]

([1]Department of Nuclear Engineering, Kyoto University, [2]Quantum Science and Engineering Center, Kyoto University)

10:05 - 10:25

"Solid-Liquid Interface Analysis with MeV-energy Heavy Ion Beams"

Toshio Seki[1,4], Makiko Fujii[2], Shunichiro Nakagawa[1], Takaaki Aoki[3,4], and Jiro Matsuo[2,4]

([1]Department of Nuclear Engineering, Kyoto University, [2]Quantum Science and Engineering Center, Kyoto University, [3]Department of Electronic Science and Engineering, Kyoto University, [4]CREST, Japan Science and Technology Agency (JST))

Session 4 Chair : Dr. Hiroshi Kudo

10:35 - 11:05 (Invited talk)

"Secondary Electron Emission from Thin Carbon Foils by Ion Beam Penetration"

Hidemi Ogawa[1], Kunikazu Ishii[1], Toshiaki Kaneko[2]

([1]Department of Physics, Nara Women's University, [2]Graduate School of Science, Okayama University of Science)

11:05 - 11:25

"Vicinage Effect on Secondary-Electron Emissions from Carbon Foils Bombarded with 62.5-keV/u C_n^+ Ions"

K. Narumi, A. Chiba, K. Yamada, S. Matoba, Y. Saitoh

(Takasaki Advanced Radiation Research Institute, Japan Atomic Energy Agency)

11:25 - 11:45

"Forward Secondary Electron Emission from Carbon Foil induced by Swift single ion and di-atom cluster ion"

Toshiaki Kaneko[1], Ryo Tanaka[1], Fuyuhito Miyahara[1], Hidemi Ogawa[2]

([1]Graduated School of Science, Okayama University of Science, [2]Graduate School of Hum. and Sci., Nara Women's University)

11:45 - 12:05

"Field Ion Microscope Observation of Organic Molecules on Tungsten Surface"

Yasuhito Gotoh, Susumu Hogyoku, and Hiroshi Tsuji

(Department of Electronic Science and Engineering, Kyoto University)

Session 5 Chair : Dr. Takanori Koshikawa

12:45 - 13:15 (Invited talk)

"Transmission secondary ions mass spectrometry of an amino acid using 5 MeV C_{60} ions"

K. Nakajima[1], K. Nagano[1], M. Suzuki[1], K. Narumi[2], Y. Saitoh[2], K. Hirata[3], and K. Kimura[1]

([1]Department of Micro Engineering, Kyoto University, [2]Takasaki Advanced Radiation Research Institute, JAEA, [3]National Metrology Institute of Japan, AIST)

13:15 - 13:35

"Enhancement of secondary ion emission from solid hydrogen films at cryogenic temperature"

Taku Suzuki

(National Institute for Materials Science)

13:35 - 13:55

"Determination of Potential Gradient near and Space Charge Potential at the Interface between Electrolyte and Electrode of Li Ion Battery by Means of ERD-RBS Techniques"

Kenji MORITA[1], Bun TSUCHIYA[2], Takehisa KATO[3], Yasutoshi IRIYAMA[3], Hideji TSUCHIDA[4], Takuya MAJIMA[4]

([1]Nagoya Industrial Science Research Institute, [2]Meijo University, [3]Nagoya University, [4]Kyoto University)

Session 6 Chair : Dr. Daiichiro Sekiba

14:05 - 14:25

"Study of hydrogen depth distributions by resonant nuclear reaction analysis toward the clarification of the reliability degradation of semiconductor devices"

Riichiro Takaishi[1], Yusuke Higashi[1], Masamichi Suzuki[1], Yuichiro Mitani[1], Mitsuhiro Tomita[1], Masuaki Matsumoto[2], Shohei Ogura[2], and Katsuyuki Fukutani[2]

([1]Corporate R&D Center, Toshiba Corporation, [2]Institute of Industrial Science, University of Tokyo)

14:25 - 14:45

"Temperature dependence of ESD rate from KBr(001) surface measured by fast proton scattering technique"

Y. Fukazawa and Y. Susuki

(Division of Science Education, Osaka Kyoiku University)

14:45 - 15:05

"Real-time observation of thermal relaxation of ion damage by synchronized positron probe analysis"

H. Tsuchida[1,2], S. Mizuno[1], H. Tsutsumi[1], A. Kinomura[3], R. Suzuki[3] and A. Itoh[1,2]

([1]Department of Nuclear Engineering, Kyoto University, [2]Quantum Science and Engineering Center, Kyoto University, [3]National Institute of Advanced Industrial Science and Technology (AIST))

The 17th Japanese Symposium on Accelerator Mass Spectrometry

Date: March 2－3 (Mon.－Thu.), 2015
Place: University Hall, University of Tsukuba

Host Organization : Tandem Accelerator Complex, University of Tsukuba
The Japan Society for AMS Research

Program

2 March 2015

Opening Remarks T. Nakamura (Nagoya University)

Session 1: Status report and development 1

(Chair: K. Sasa, H. Matsumura)

1－1 Status and Application of AMS System at Nagoya University (2014) : T. Nakamura (Nagoya University)

1－2 Installation of compact AMS to the University of Tokyo : M. Yoneda (The University of Tokyo)

1－3 Development of ^{236}U-AMS – Identification of interference components : K. Nakashoji (The University of Tokyo)

1－4 Development of ^{36}Cl-AMS using the PHITS code and measurement of cosmogenic nuclides : D. Izumi (University of Tsukuba)

1－5 Development of GC-AMS system and performance of automatic sample preparation system for ^{14}C-AMS at the University of Tsukuba : T. Matsunaka (University of Tsukuba)

Session 2: Application 1

(Chair: A. Sakaguchi)

2－1 The variation of ^{129}I deposition in Tsukuba region : M. Watanabe (University of Tsukuba)

2－2 Behavior of dissolved radionuclides and ions in riverine water after the FDNPP accident : R. Tomita (University of Tsukuba)

2－3 Study of iodine dynamics in soil by analysis of ^{129}I/^{127}I ratio : W. Kijima (The University of Tokyo)

2－4 The speciation analysis for iodine in seawater : E. Tanaka (The University of Tokyo)

2－5 Comparison of $^{129}I/^{127}I$ ratio between marine fishes and seawater : H. Kusuno (The University of Tokyo)

Session 3: Application 2

(Chair: K. Sueki)

3－1 Establishment of the estimation method of the date of birth by using tooth enamel, root organic and inorganic matter of Japanese : K. Kunita (Nagoya University)

3－2 High precision radiocarbon dating of charred materials using ABOx-SC treatment
S. Tomiyama (Nagoya University)

3－3 Rapid change of sedimentation rate from Lake Baikal sediment core corresponding with the global climate warming
F.W. Nara (Tohoku University)

3－4 Geochronology and geochemistry of past tsunami sediments
T. Watanabe (Tohoku University)

Special lecture 1

(Chair: T. Nakamura)

S－1 Introduction of KIGAM AMS Lab. and Related Facilities
W. Hong (KIGAM)

Poster Session

P－1 An attempt on ^{14}C dating of a cremated bone
H. Mukumoto (Nagoya University)

P－2 Design of the negative ion cooler
Y. Miyake (The University of Tokyo)

P－3 Development of degradation method of radionuclide in soil using pressure vessel
M. Honda (University of Tsukuba)

P－4 Determination of ultra-low ^{129}I and ^{99}Tc in soil samples by Triple Quadrupole ICP-MS
M. Honda (University of Tsukuba)

P－5 ^{14}C age at the early Sporer minimum of tree-ring from the northern Japan
M. Hakozaki (Nagoya University)

P－6 Temporal changes in volcanic activity and iodine isotopic ratio at Zao volcano
T. Matsunaka (University of Tsukuba)

P－7 Basic knowledge for development of ^{90}Sr-AMS
Y. Satou (University of Tsukuba)

P－8 Current Status of System Technology in the JAEA-AMS-TONO (2014)
A. Matsubara (JAEA)

P－9 Continuous research of ^{129}I contamination in the chemical sample preparation room for AMS
M. Matsumura (University of Tsukuba)

P－10 Possibility of radiocarbon dating to bronze implement and application to a bronze bell called Dojoji Kanemeki Doutaku
H. Oda (Nagoya University)

P－11 ^{236}U in the pan-Japan Sea area
A. Sakaguchi (University of Tsukuba)

3 March 2015

Session 4: Status report and development 2

(Chair: T. Matsunaka, A. Matsubara)

4－1 Present status of the JAEA-AMS-TONO (2014)
Y. Saito-Kokubu (JAEA)

4－2 Status report of MALT, The University of Tokyo
H. Matsuzaki (The University of Tokyo)

4－3 Installation Status and Future Prospects of the 6 MV AMS system at the University of Tsukuba
K. Sasa (University of Tsukuba)

4－4 Current status of the Compact AMS system at Paleo Lab Co., Ltd. (2014)
M. Sato (Paleo Labo Co., Ltd.)

4－5 Status report of Single Stage AMS at Atmosphere and Ocean Research Institute, The University of Tokyo

Y. Miyairi (The University of Tokyo)

Special lecture 2

(Chair: K. Sasa)

S－2 The Contribution of AMS to the Study of West Asian Archaeology
A. Tsuneki (University of Tsukuba)

Special lecture 3

(Chair: H. Matsuzaki)

S－3 The Installation of the 6 MV tandem AMS/IBA accelerator recently installed at Tsukuba University
M.V. Mores (NEC)

Session 5: Application 3

(Chair: T. Watanabe, M. Hakozaki)

5－1 Temporal change in bomb-produced radiocarbon in the North Pacific in the past two decades derived from repeat hydrography
Y. Kumamoto (JAMSTEC)

5－2 Contribution of Dead carbon source to fluctuate DI^{14}C in Lake Biwa water
Y. Miyata (Kanazawa University)

5－3 RICE-W (Radiocarbon Intercomparison on Chemical Experiments, Water series) program-An interim report-
H.A. Takahashi (AIST)

5－4 The indirect radiocarbon dating using microscope observation and bibliographical consideration of calligraphy
H. Oda (Nagoya University)

5－5 Distribution of ^{129}I in the Arctic and North Pacific Ocean
H. Nagai (Nihon University)

Closing Remarks K. Sasa (University of Tsukuba)

Facility tour (6 MV AMS system, Sample preparation room)

8.

LIST OF PERSONNEL

Tandem Accelerator Complex

E. Kita	Director, Professor
K. Sasa	Associate Professor
D. Sekiba	Lecturer
T. Moriguchi	Assistant Professor
H. Oshima	Electrical Engineer
Y. Tajima	Mechanical Engineer
S. Ishii	Mechanical Engineer
T. Takahashi	Electrical Engineer
Y. Yamato	Electrical Engineer
T. Matsunaka	Research Fellow
M. Matsumura	Research Supporter
M. Ohyama	Administrative Staff
N. Yamada	Administrative Staff
H. Muromachi	Administrative Staff

Research Members[1]

Inst. of Physics

I. Arai	K. Sasa	D. Nagae	A.Ozawa

Inst. of Applied Physics

K. Akimoto	S. Selvakumar	E. Kita	M. Minagawa
D. Sekiba	T. Suemasu	S. Tomita	A. Uedono
H. Yanagihara	Y. Watahiki		

Inst. of Materials Science

T. Kondo	M. Takahashi

Inst. of Geoscience

M. Kurosawa

Inst. of Chemistry

K. Sueki	A. Sakaguchi

Staff of Open Advanced Facilities Initiative

[1] The “research members” include the authors and coauthors within 5 years back from this fiscal year, as well as the members of research projects running at UTTAC.

H. Kudo	H. Naramoto	M. Sataka	A. Yamazaki
H. Muromachi			

Graduate students

Doctoral Programs of Pure and Applied Science

Y. Abe	S. Fukuoka	I. Harayama	Y. Ishibashi
K. Kurita	S. Kimura	M. Mukai	M. Honda
Y. Satou			

Master's Programs of Pure and Applied Science

F. Arai	H. Alima	R. Aoyama	A. Horiuchi
D. Izumi	Y. Ichikawa	Y. Liu	S. Maeda
K. Sawahata			

Undergraduates

E. Noguchi	T. Tamura	R. Tomita	M. Watanabe

Scientific Gutests and Fellows

K. Awazu	National Institute of Advanced Industrial Science and Technology (AIST)
M. Fujimaki	National Institute of Advanced Industrial Science and Technology (AIST)
Y. Tosaki	National Institute of Advanced Industrial Science and Technology (AIST)
T. Hayakawa	Japan Atomic Energy Agency (JAEA)
T. Shizuma	Japan Atomic Energy Agency (JAEA)
S. Kubono	Center for Nuclear Study, the University of Tokyo (CNS)
A. Sato	Osaka University
A. Yamamoto	High Energy Accelerator Research Organization (KEK)
T. Adachi	High Energy Accelerator Research Organization (KEK)
M. Yoshida	High Energy Accelerator Research Organization (KEK)
N. Kawamura	High Energy Accelerator Research Organization (KEK)
K. Shimomura	High Energy Accelerator Research Organization (KEK)
P. Strasser	High Energy Accelerator Research Organization (KEK)
T. Nakamoto	High Energy Accelerator Research Organization (KEK)
M. Iio	High Energy Accelerator Research Organization (KEK)
K. Yoshimura	High Energy Accelerator Research Organization (KEK)
H. Matsumura	High Energy Accelerator Research Organization (KEK)
N. Kinoshita	SHIMIZU Corporation